© 2014. Published by The Company of Biologists Ltd | Development (2014) 141, 3399-3409 doi:10.1242/dev.106773

RESEARCH ARTICLE

Heterotrimeric Go protein links Wnt-Frizzled signaling with ankyrins to regulate the neuronal microtubule cytoskeleton

Anne-Marie Lüchtenborg[1,2], Gonzalo P. Solis[1], Diane Egger-Adam[2], Alexey Koval[1], Chen Lin[1,2], Maxime G. Blanchard[1], Stephan Kellenberger[1] and Vladimir L. Katanaev[1,2,*]

ABSTRACT

Drosophila neuromuscular junctions (NMJs) represent a powerful model system with which to study glutamatergic synapse formation and remodeling. Several proteins have been implicated in these processes, including components of canonical Wingless (*Drosophila* Wnt1) signaling and the giant isoforms of the membrane-cytoskeleton linker Ankyrin 2, but possible interconnections and cooperation between these proteins were unknown. Here, we demonstrate that the heterotrimeric G protein Go functions as a transducer of Wingless-Frizzled 2 signaling in the synapse. We identify Ankyrin 2 as a target of Go signaling required for NMJ formation. Moreover, the Go-ankyrin interaction is conserved in the mammalian neurite outgrowth pathway. Without ankyrins, a major switch in the Go-induced neuronal cytoskeleton program is observed, from microtubule-dependent neurite outgrowth to actin-dependent lamellopodial induction. These findings describe a novel mechanism regulating the microtubule cytoskeleton in the nervous system. Our work in *Drosophila* and mammalian cells suggests that this mechanism might be generally applicable in nervous system development and function.

KEY WORDS: *Drosophila*, Neuromuscular junction, Wnt, Frizzled, G protein, Ankyrin, Microtubules

INTRODUCTION

Go is the most abundant heterotrimeric G protein in the central nervous system of both vertebrates and invertebrates (Sternweis and Robishaw, 1984; Wolfgang et al., 1990). It is the immediate transducer of a number of G protein-coupled receptors (GPCRs), including receptors of the Frizzled (Fz) family (Egger-Adam and Katanaev, 2008). In *Drosophila*, Go is involved in transduction of the Wingless (Wg; *Drosophila* Wnt1) signal (Katanaev et al., 2005). Go can physically interact with Fz proteins, and binding of Wnt ligands to Fz induces an exchange of the guanine nucleotide on the Gα subunit of Go (Gαo) (Koval and Katanaev, 2011). The initial heterotrimeric complex then dissociates into free Gα-GTP and the Gβγ dimer; both are involved in downstream signaling. The intrinsic GTPase activity of Gα leads to hydrolysis of GTP to GDP; the resultant Gα-GDP can continue to signal or associates back with Gβγ to bind GPCRs (Gilman, 1987; Katanaev, 2010).

[1]Department of Pharmacology and Toxicology, Faculty of Biology and Medicine, University of Lausanne, Rue du Bugnon 27, Lausanne 1005, Switzerland. [2]Department of Biology, University of Konstanz, Universitätsstrasse 10, Box 643, Konstanz 78457, Germany.

*Author for correspondence (vladimir.katanaev@unil.ch)

Received 4 December 2013; Accepted 9 July 2014

The evolutionarily conserved Wg pathway is important for numerous developmental programs and cellular processes (Logan and Nusse, 2004). In the nervous system of *Drosophila*, Wg signaling is involved in the formation of neuromuscular junctions (NMJs) (Packard et al., 2002; Miech et al., 2008). Being a glutamatergic synapse, the *Drosophila* NMJ provides a useful experimental model with which to study mammalian central nervous system synapses, their formation and remodeling (Collins and DiAntonio, 2007). The *Drosophila* NMJ is a beads-on-a-string-like structure that is formed at the axon terminus and is composed of distinct circular structures – the synaptic boutons – which contain active zones for neurotransmitter release. During growth, the NMJ is subject to remodeling to build additional synapses on the growing muscle, which is achieved by the formation of new boutons as well as by budding off from the existing boutons (Zito et al., 1999). These processes require cytoskeletal rearrangements (Roos et al., 2000) and depend on the proper response to the Wg ligand, which is produced presynaptically (Packard et al., 2002; Korkut et al., 2009).

In canonical Wnt signaling, binding of the ligand to Fz and a co-receptor, LRP5/6 (Arrow in *Drosophila*), leads to reorganization of the cytoplasmic β-catenin-destruction machinery, which contains, among other proteins, glycogen synthase kinase 3β [GSK3β; Shaggy (Sgg) in *Drosophila*]. Receptors (Fz and LRP5/6) are activated by Wnt signal to disassemble the destruction complex, leading to the stabilization of β-catenin, its translocation into the nucleus and the induction of transcription of Wnt target genes (Logan and Nusse, 2004).

However, this canonical pathway is not active in the *Drosophila* NMJ. Instead, on the postsynaptic side of the NMJ the Wg signal is transduced via endocytosis and cleavage of Frizzled 2 (Fz2) and nuclear import of its C-terminal fragment, which is required for the proper transcription-dependent establishment of postsynaptic densities (Mathew et al., 2005; Mosca and Schwarz, 2010). On the presynaptic side, the Wg pathway does not involve β-catenin nor transcription but does require inhibition of Sgg activity (Miech et al., 2008); Sgg in the presynapse is proposed to regulate the stability of the microtubule cytoskeleton through phosphorylation of the microtubule-binding protein Futsch (*Drosophila* MAP1B) (Franco et al., 2004; Gogel et al., 2006; Miech et al., 2008). The microtubule cytoskeleton in the presynaptic NMJ cell is also under the control of Ankyrin 2 (Hortsch et al., 2002; Koch et al., 2008; Pielage et al., 2008).

Ankyrins (Ank) are highly abundant modular proteins that mediate protein-protein interactions, mainly serving as adaptors for linking the cytoskeleton to the plasma membrane (Bennett and Baines, 2001). Mammalian genomes encode three Ank genes [*AnkR* (*Ank1*), *AnkB* (*Ank2*) and *AnkG* (*Ank3*)], whereas *Drosophila* has two [*Ank1* (also known as *Ank* – FlyBase) and *Ank2*] (Dubreuil and Yu, 1994; Bouley et al., 2000). *Ank2* is expressed exclusively in neurons and exists in several splicing variants (Koch et al., 2008;

Development (2014) 141, 3399-3409 doi:10.1242/dev.106773

Pielage et al., 2008). The larger isoforms (Ank2M, Ank2L and Ank2XL) are localized to axons and play important roles in NMJ formation and function (Hortsch et al., 2002; Koch et al., 2008; Pielage et al., 2008). The C-terminal part of Ank2L can bind to microtubules (Pielage et al., 2008). Despite the well-established role of Ank2 in NMJ formation, its function has been considered somewhat passive and its mode of regulation has not been clarified. Here, we show that Gαo binds to Ank2 and that these proteins and the Wg pathway components Wg, Fz2, and Sgg jointly coordinate the formation of the NMJ. We also show that the functional Gαo-Ank interaction is conserved from insects to mammals.

RESULTS

Go is abundant in the NMJ and is required for normal NMJ physiology

Since Go is abundant in neurons and is involved in Fz signaling, we investigated its presence and function in the NMJ. To visualize the synaptic boutons, we used the postsynaptic marker CD8-GFP-Sh (Zito et al., 1999) or Discs large (Dlg; Dlg1 – FlyBase) (Guan et al., 1996) (Fig. 1A; supplementary material Fig. S1A). For the presynaptic side we used the marker Bruchpilot (Brp) (Wagh et al., 2006) (Fig. 1B) or performed anti-HRP staining (Jan and Jan, 1982) (supplementary material Fig. S1A,B). Using two different anti-Gαo antibodies (see Materials and Methods), we found strong anti-Gαo staining in boutons as well as in axons (Fig. 1C; supplementary material Fig. S1A-D). Comparison of Gαo staining with the markers revealed that Gαo is expressed in the presynaptic cell, overlapping with Brp (Fig. 1D-F; supplementary material Fig. S1C,D) and anti-HRP (supplementary material Fig. S1A,B). This is particularly evident at high magnification, which shows the anti-Gαo staining encircled by postsynaptic Dlg and CD8-GFP-Sh (supplementary material Fig. S1B,D). Interestingly, this pattern is different from that of anti-Gβ13F staining, which recognizes the major Gβ subunit in *Drosophila* (Katanayeva et al., 2010): this pan-G protein Gβ subunit shows both pre- and postsynaptic staining, the latter being even broader than the CD8-GFP-Sh pattern (supplementary material Fig. S1H) or that of anti-Dlg (not shown). A role of Gβ13F both in the nervous system (Schaefer et al.,

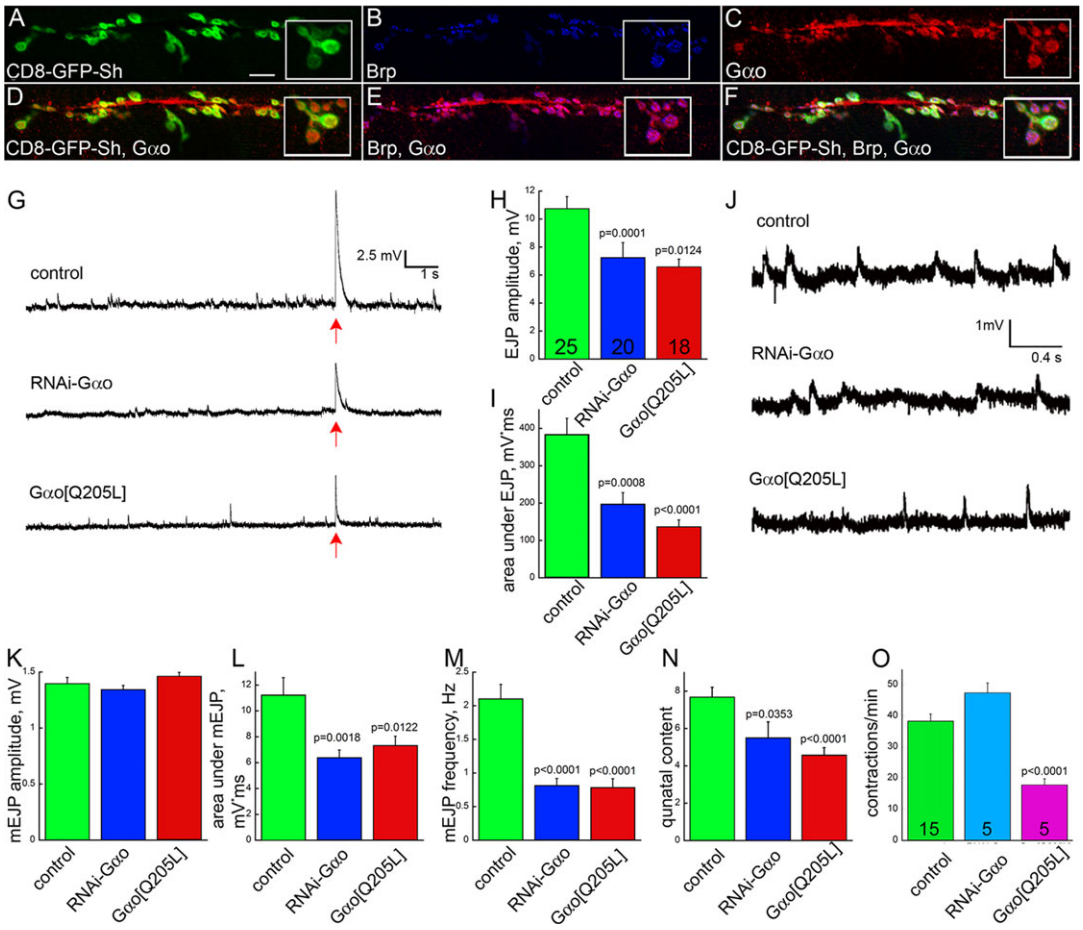

Fig. 1. Gαo is expressed in the presynaptic cell of the NMJ and is required for normal NMJ physiology. (A-F) Gαo (red in C-F) is expressed in the presynaptic side of the NMJ and is barely detected postsynaptically, as judged by colocalization with Brp (blue in B,E,F) but only partial overlap with CD8-GFP-Sh (green in A,D,F). Insets are enlargements of the terminal boutons. Scale bar: 10 μm. (G) Representative traces of spontaneous NMJ activity and one illumination-evoked action potential [arrow indicates the time of illumination; arrow thickness is in scale with the length of illumination (20 ms)] recorded from control (*OK371-Gal4;UAS-ChR2*), RNAi-Gαo (*OK371-Gal4;UAS-ChR2/UAS-RNAi-Gαo*) and Gαo[Q205L] (*OK371-Gal4;UAS-ChR2/UAS-Gαo[Q205L]*) larvae. (H,I) Quantification of amplitude (H) and area under the peak (I) of excitatory junctional potentials (EJPs) from individual muscles from the three genotypes; the number of muscles analyzed is shown in H. (J) Higher magnification of a region in G to show representative traces of spontaneous NMJ activity. (K-M) Quantification of amplitude (K), area (L) and frequency (M) of spontaneous miniature EJPs (mEJPs) of the three genotypes, recorded in the same muscles as in H. (N) Quantal content of the three genotypes calculated as EJP/mEJP. (O) Locomotion activity measured as the number of contractions per minute of third instar larvae of the three genotypes; the number of animals tested is shown in the bars. *P*-values are shown where the observed differences between the mutant and control conditions are statistically significant ($P<0.05$). Error bars indicate s.e.m.

Development (2014) 141, 3399-3409 doi:10.1242/dev.106773

2001) and in muscles (Schnorrer et al., 2010) has been described previously.

To investigate the physiological importance of Gαo in the NMJ, we perturbed Gαo activity in the synapse. Gαo was modulated by the presynaptic expression of two previously tested *UAS* constructs: *RNAi-Gαo*, which downregulates Gαo (Purvanov et al., 2010) (see supplementary material Fig. S1I-K for the efficiency of downregulation); and *Gαo[Q205L]*, which is a constitutively active mutant form that is unable to hydrolyze GTP (Katanaev et al., 2005; Kopein and Katanaev, 2009). These two constructs were driven by the motoneuron driver *OK371-Gal4* (Mahr and Aberle, 2006). Excitatory junctional potentials (EJPs) were induced by light-activated channelrhodopsin-2 (Schroll et al., 2006) (see Materials and Methods). Analysis of EJPs in the NMJ of the control, *RNAi-Gαo* and *Gαo[Q205L]* larvae revealed a marked reduction in EJP amplitude and width with each perturbation of Gαo function (Fig. 1G-I).

We also analyzed spontaneous NMJ activity. Although the amplitude of miniature excitatory junctional potentials (mEJPs) was almost identical in the three conditions, their duration and frequency were strongly reduced upon overactivation and downregulation of Gαo (Fig. 1J-M). Decreased mEJP frequency with largely unperturbed mEJP amplitude suggests that motoneuron-specific modulation of Gαo function mainly induces presynaptic defects. The ratio of EJP to mEJP amplitudes provides the junctional quantal content. This measure of synaptic efficacy is significantly reduced in both mutant conditions (Fig. 1N), suggesting that the number of synaptic vesicles released upon stimulation is decreased in the *RNAi-Gαo* and *Gαo[Q205L]* conditions. These data might indicate that the number of mature boutons or their functionality is decreased by unbalancing Gαo activity in the presynapse. Additionally, we found that in *Gαo[Q205L]* larvae the overall crawling capacity was also perturbed (Fig. 1O).

Aberrant Gαo activity leads to morphological defects in the NMJ similar to those associated with abnormal Wg-Fz2 signaling

To examine why aberrant NMJ physiology accompanies reduced or increased Gαo activity, we performed immunostaining and a morphological investigation of the mutant synapses. We found reduced numbers of boutons in *RNAi-Gαo*-expressing NMJs (Fig. 2A). This reduction was rescued by re-expression of Gαo (but not of an unrelated protein; supplementary material Fig. S2A). Pertussis toxin (Ptx) is a specific inhibitor of Gαo in *Drosophila*, uncoupling it from cognate GPCRs (Katanaev and Tomlinson, 2006b), and its expression in motoneurons led to a ~50% reduction in the number of boutons (Fig. 2A). In addition to *OK371-Gal4*, other drivers such as the pan-neuronal *elav-Gal4* (Luo et al., 1994)

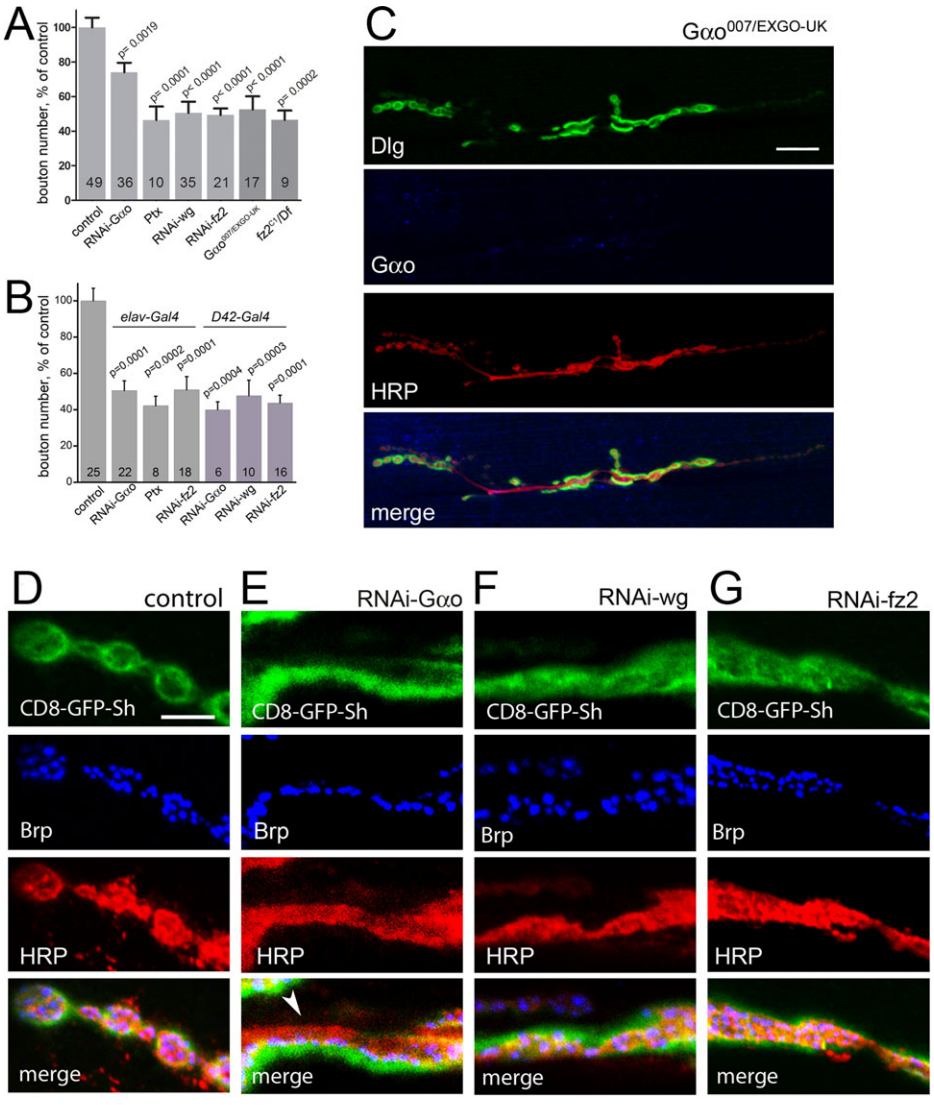

Fig. 2. Gαo is required for NMJ formation, similar to Wg and Fz2. (A) Quantitative analysis of bouton number on muscle 6/7. Presynaptic downregulation of Gαo, Wg and Fz2 with the driver *OK371-Gal4*, expression of Ptx, as well as genetic removal of *Gαo* or *Fz2* lead to a significant decrease in bouton number compared with the wild type (control). Data are represented as percentage of control; the number of NMJs analyzed for each genotype is shown in each bar; *P*-values compared with the control are indicated; error bars indicate s.e.m. (B) Downregulation of Gαo or Fz2 and expression of Ptx with the pan-neuronal driver *elav-Gal4* similarly decrease bouton numbers. The same effect is observed when RNAi against *Gαo*, *wg* or *fz2* is driven with motoneuron-specific *D42-Gal4*. (C) Genetic removal of *Gαo* leads to a strong reduction in bouton number and aberrant NMJ morphology (compare with Fig. 1A-F). Anti-Gαo staining (blue) confirms loss of the proteins; the remaining signal is non-specific. (D-G) Presynaptic downregulation of Gαo, Wg or Fz2 results in malformed boutons. Displayed is a detail of the NMJ on muscle 6/7 that is stained with anti-HRP to visualize the presynaptic cell membrane in red, with anti-Brp to stain the active zones in blue, and the postsynaptic marker CD8-GFP-Sh in green. All mutant genotypes lead to the development of elongated structures with defective overlap of pre- and postsynapse (E, arrowhead) instead of the circular postsynaptic boutons with postsynaptic staining encircling presynaptic staining as in the wild type (D). Scale bars: 20 µm in C; 5 µm in D-G.

Development (2014) 141, 3399-3409 doi:10.1242/dev.106773

(see supplementary material Fig. S1K,L) and the motoneuron-specific *D42-Gal4* (Parkes et al., 1998), when used to target Gαo through expression of RNAi or Ptx, also led to a substantial decrease in bouton numbers (Fig. 2B). The Wg-secreting type Ib boutons (Packard et al., 2002) appeared more severely affected by Gαo perturbations than type Is boutons (supplementary material Fig. S2B). Finally, genetic removal of *Gαo* replicated the Gαo downregulation data (Fig. 2A), resulting in a strong reduction in bouton numbers and aberrant NMJ morphology (Fig. 2C, compare with Fig. 1A-F); presynaptic re-expression of Gαo was able to rescue the $Gαo^{-/-}$ defects (supplementary material Fig. S2A). Thus, Gαo is presynaptically required for proper NMJ development. The decrease in bouton number induced by *RNAi-Gαo* parallels the reduced electric activity of the mutant NMJ (Fig. 1).

Gαo is a transducer of Fz2 (Katanaev et al., 2005; Katanaev and Tomlinson, 2006a; Purvanov et al., 2010), and the Wg-Fz2 pathway has been implicated in NMJ formation. In accordance with previous observations (Packard et al., 2002; Mathew et al., 2005), presynaptic downregulation of Wg (supplementary material Fig. S1M,N) or genetic loss of *fz2* led to a strong decrease in bouton numbers (Fig. 2A,B). Fz2 is present both pre- and postsynaptically (Packard et al., 2002), and the importance of the postsynaptic Fz2 for NMJ development has been demonstrated (Mathew et al., 2005; Mosca and Schwarz, 2010). Here we show that presynaptic Fz2 is also crucial for the NMJ, as specific presynaptic downregulation of Fz2 by various drivers (supplementary material Fig. S1O,P) reduces bouton numbers to the levels found in *fz2* null mutants (Fig. 2A,B). We also tested the ability of presynaptic re-expression of *fz2* to rescue bouton numbers in the *fz2* null background, and observed a complete rescue of bouton number (supplementary material Fig. S1Q,R), analogous to the rescue by postsynaptic *fz2* expression in *fz2* mutants (supplementary material Fig. S1Q) (Mathew et al., 2005), providing evidence for the important neuronal role of the Wg-Fz2 pathway in the NMJ.

This quantitative analysis was corroborated with morphological studies. Genetic removal of *Gαo* (Fig. 2C), expression of Ptx (supplementary material Fig. S1S) or silencing of *Gαo* resulted in clear morphological changes in the NMJ (Fig. 2D,E), similar to those previously described for *wg* loss-of-function mutations (Packard et al., 2002) and identical to those induced by downregulation of Wg and Fz2 (Fig. 2F,G), in which tube-like structures could be observed in the mutant NMJs instead of the normal separate circular boutons, often with diffuse presynaptic Brp and anti-HRP staining.

We next examined the effect of overexpression of different forms of Gαo in the presynapse. In addition to the constitutively GTP-loaded Gαo[Q205L] form used above, we also overexpressed wild-type Gαo and the Gαo[G203T] mutant (Katanaev et al., 2005), which has a reduced affinity for GTP (supplementary material Fig. S2C) but does not behave as a dominant-negative construct (see Discussion). Expression of all three *Gαo* forms with *OK371-Gal4* induced the formation of smaller and more compact boutons as compared with the normal NMJ (Fig. 3A-C). This morphological change was also observed when *wg* (Packard et al., 2002; Miech et al., 2008) or *fz2* was overexpressed presynaptically (Fig. 3D). Overexpression of *fz1* (also known as *fz* – FlyBase), by contrast, did not affect NMJ morphology (not shown). To further verify the influence of Wg signaling on NMJ formation we expressed *RNAi-sgg* in the presynapse, where Sgg localizes (Franco et al., 2004; Miech et al., 2008). Downregulation of this destruction complex protein resulted in a phenotype similar to that of overexpression of *Gαo* or *fz2* (Fig. 3E).

Quantitative analysis showed that overexpression of *Gαo* and its mutant forms, as well as overexpression of *wg* or *fz2* (but not *fz1*) and downregulation of *sgg*, significantly increased the total number of boutons and their density (the number of boutons per µm NMJ length; Fig. 3F; supplementary material Fig. S2D,E). Expression of different dominant-negative constructs of Sgg (SggDN) presynaptically was previously reported to increase bouton number, whereas postsynaptic expression of SggDN had no effect on NMJ formation (Franco et al., 2004; Miech et al., 2008). As the neurotransmitter release properties of Gαo[Q205L] NMJ are reduced (Fig. 1), the increased numbers of boutons observed upon overactivation of the Wnt pathway, as described here, might indicate

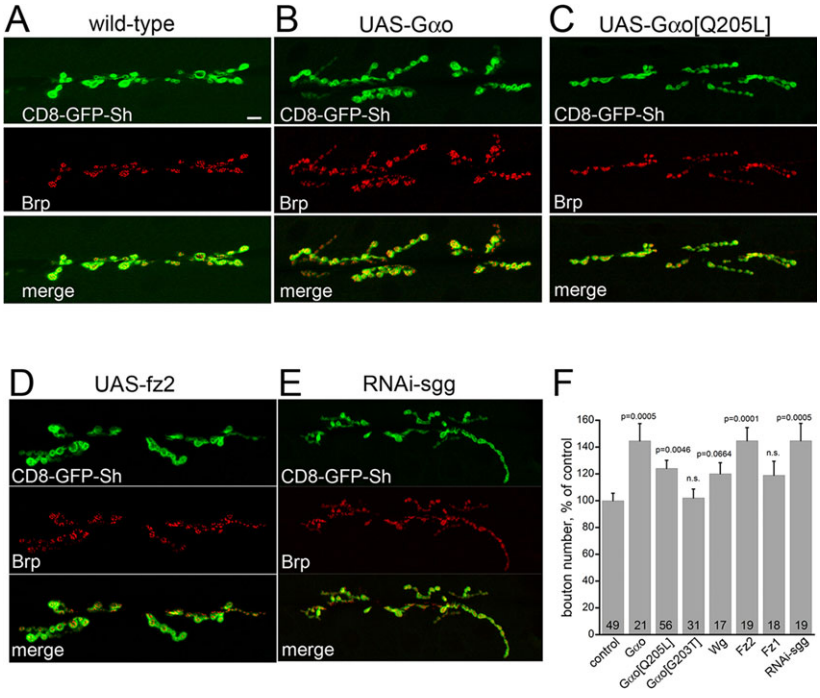

Fig. 3. Overexpression of Gαo or Fz2 in the presynaptic cell, as well as downregulation of Sgg, stimulates bouton formation in NMJ. (A) Wild-type NMJ stained for the presynaptic marker Brp (red); the postsynaptic cell is visualized by CD8-GFP-Sh (green). (B,C) Overexpression of Gαo and its mutant GTP-loaded form (Gαo[Q205L]) in the presynaptic cell leads to enhanced bouton formation. (D,E) Overexpression of *fz2* or expression of *RNAi-sgg* produces similar phenotypes. (F) Quantification of bouton numbers in the different genotypes (shown as in Fig. 2A). n.s., not significant (P>0.05). Scale bar: 10 µm.

Development (2014) 141, 3399-3409 doi:10.1242/dev.106773

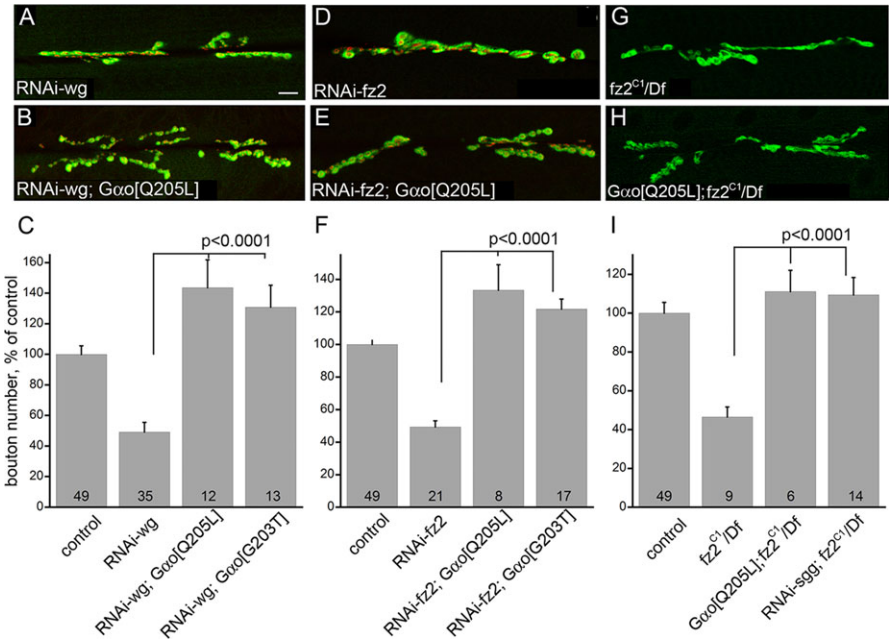

Fig. 4. Gαo acts downstream of Wg-Fz2 in the NMJ. Expression of the GDP-loaded and GTP-loaded mutant forms of Gαo (Gαo[G203T] and Gαo[Q205L], respectively) rescues the *RNAi-wg* (A-C), *RNAi-fz2* (D-F) and the *fz2* mutant (G-I) phenotypes. Brp (red) and CD8-GFP-Sh (green, A,B,D,E) or Dlg (G,H) visualize pre- and postsynaptic compartments, respectively. Quantification of bouton numbers (C,F,I) is as in Fig. 2A; *RNAi-sgg* also rescues the *fz2* null phenotype (I). Scale bar: 10 µm.

that these boutons are non-functional or that Gαo overactivation interferes with proper synaptic transmission.

Cumulatively, these findings suggest that Gαo acts as a transducer of the Wg-Fz2 pathway in the NMJ. Formally, Gαo might alternatively regulate Fz2 abundance in the NMJ. However, no discernible changes in Fz2 levels in the NMJ could be observed in the different *Gαo* backgrounds (supplementary material Fig. S2G).

Gαo is a transducer of Wg and Fz2 in the NMJ

To unequivocally demonstrate that Gαo is a downstream transducer of the Wg-Fz2 signal in the NMJ, we performed epistasis experiments among these proteins. Remarkably, regardless of its nucleotide state, overexpression of *Gαo* in the motoneurons was effective in rescuing the phenotypes obtained by neuronal downregulation of *wg* or *fz2* using RNAi constructs (Fig. 4A-F). In all cases, the morphology of the NMJ resembled that observed in *Gαo*-overexpressing larvae (Fig. 3B,C). The morphological rescue was confirmed by quantitative analysis of bouton numbers (Fig. 4C,F). We further confirmed the epistasis between Gαo and Fz2 using genetic null alleles of *fz2*. Complete loss of Fz2 substantially alters the morphology of the NMJ and decreases bouton numbers (Fig. 4G,I). These phenotypes could be completely rescued by neuronal expression of *Gαo[Q205L]* (Fig. 4H,I). The same rescue of the *fz2* null could be achieved by *RNAi-sgg* (Fig. 4I).

Thus, Gαo acts as a (presumably immediate) transducer of Wg-Fz2 signaling in the NMJ. The similar efficiencies of the GTP- and GDP-loaded forms of Gαo in executing the Wg-Fz2 signal suggest that the molecular target(s) of Gαo in this signaling pathway does not discriminate between the two nucleotide states of the G protein.

Ank2 physically binds to and acts downstream of Gαo in the *Drosophila* NMJ

To identify potential Gαo target proteins, we performed a yeast two-hybrid screen with a *Drosophila* head cDNA library as prey and Gαo as bait (Kopein and Katanaev, 2009). We identified three clones of Ank2 interacting with Gαo with high confidence. The interaction site could be narrowed to amino acids 47-123 of Ank2 (Fig. 5A; see Materials and Methods). In order to confirm the Gαo-Ank2 interaction and to investigate its dependence on guanine nucleotides, we bacterially expressed and purified a truncated maltose-binding protein (MBP)-tagged Ank2 construct (Ank2_12) that consisted of the first 12 ankyrin repeats containing the Gαo binding site (see supplementary material Fig. S3A for characterization of the resulting recombinant protein). We additionally purified highly active recombinant Gαo (Kopein and Katanaev, 2009). In the pull-down experiments, we found that Gαo and Ank2_12 efficiently interacted with each other, supporting the yeast two-hybrid data (Fig. 5B). The GDP- and GTPγS-loaded forms of Gαo were equally efficient in Ank2 binding, expanding the list of Gαo target proteins that do not discriminate between the two nucleotide forms of this G protein (Katanaev, 2010). Importantly, preincubation of Gαo with Gβγ dramatically reduced the amounts of Gαo pulled down by Ank2_12 (Fig. 5C, top). Furthermore, the small amounts of Gαo still interacting with Ank2_12 in this experiment remained Gβγ free, as no Gβγ was detected in Ank2 pull-downs (Fig. 5C, bottom). Thus, Ank2 behaves as a true effector of Gαo, interacting with the monomeric Gβγ-free form of this G protein.

The described (Koch et al., 2008; Pielage et al., 2008; see also Fig. 5D) phenotypes of *Ank2* mutants resemble those that we see upon RNAi-mediated presynaptic downregulation of *Gαo*, *fz2* and *wg*. To test whether Ank2 is epistatic to Wg-Fz2-Gαo signaling, we overactivated this pathway at different levels in the *Ank2* null background. Overexpression of *Gαo* or *Gαo[Q205L]* or downregulation of *sgg* failed to rescue the bouton morphology of the *Ank2* nulls (Fig. 5D-G), and the bouton density remained severely decreased (Fig. 5H), suggesting that Ank2 is epistatic to both Gαo and Sgg in synapse formation. However, Gαo could still localize to the NMJ despite Ank2 absence (supplementary material Fig. S3C), demonstrating that Ank2 does not merely control Go localization in the NMJ.

We also expressed RNAi against *Ank2L* (Pielage et al., 2008) with *OK371-Gal4*, producing morphological defects similar to those resulting from downregulation of *wg*/*fz2*/*Gαo* (Fig. 5I). Overexpression of *wg* or *fz2* in the *RNAi-Ank2L* background failed to restore or improve the synaptic morphology and bouton numbers of *Ank2* downregulation (Fig. 5J,K). Fz2 faithfully localizes to the NMJ despite reduced Ank2 levels (Fig. 5K; supplementary material Fig. S2G), again arguing that Ank2 does not simply regulate the

Development (2014) 141, 3399-3409 doi:10.1242/dev.106773

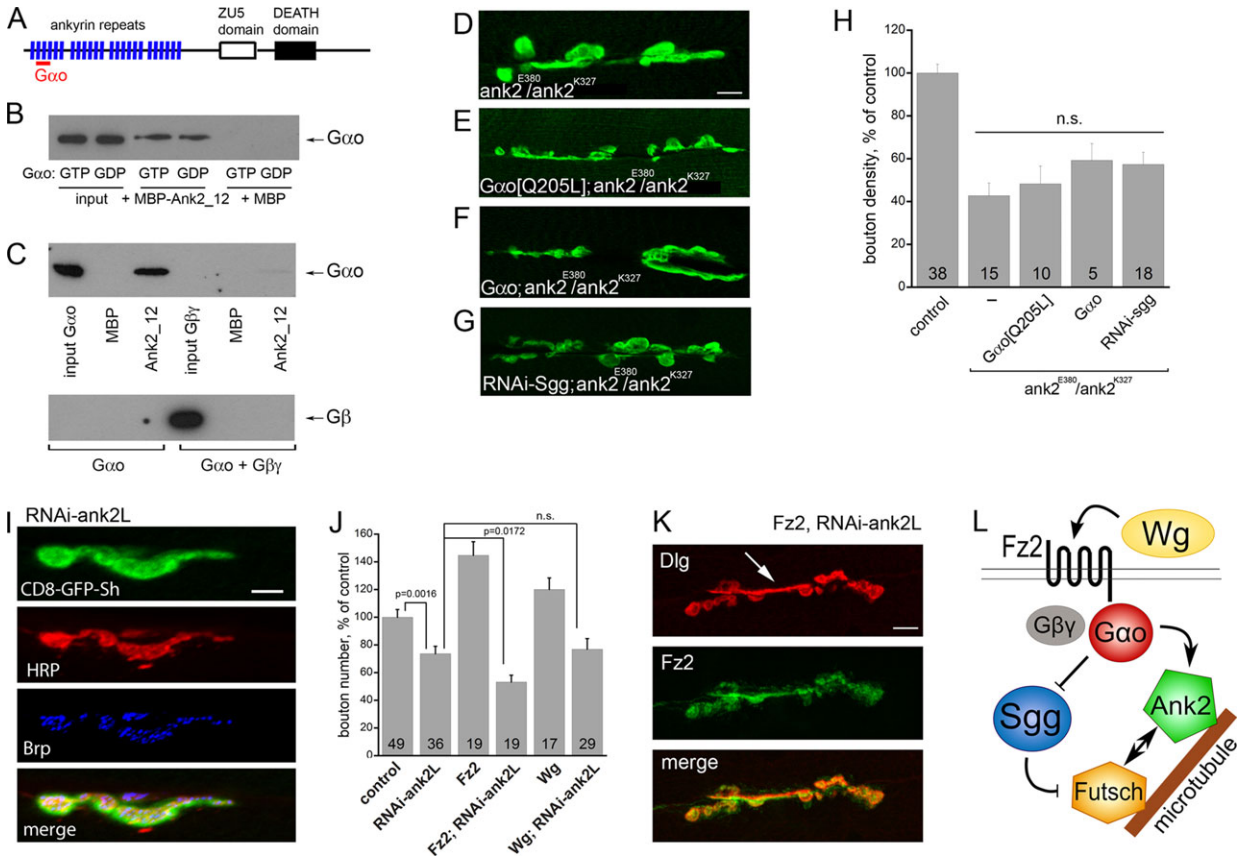

Fig. 5. Ank2 acts downstream from Gαo and physically interacts with it. (A) Structure of Ank2, displaying the four ankyrin-repeat domains (each composed of six ankyrin repeats), the ZU5 (spectrin binding) and the DEATH domains. The Gαo binding site detected in the yeast two-hybrid screen is located between amino acids 47 and 123 (red bar). (B) Pull-down experiments between Gαo and truncated Ank2 (Ank2_12, consisting of the first 12 ankyrin repeats) confirm the yeast two-hybrid interaction. Gαo efficiently interacts with Ank2 regardless of the guanine nucleotide with which it is preloaded (GDP or GTPγS). Maltose-binding protein (MBP) is the negative control showing no interaction with Gαo. (C) The binding between Gαo and Ank2 is outcompeted by Gβγ: preincubation of Gαo with equimolar Gβγ drastically diminishes the amounts of Gαo competent to interact with Ank2_12; Gβγ is not pulled down by Ank2. The bottom western blot panel is intentionally overexposed to show that no Gβγ is pulled down by Ank2. (D-G) *Ank2* null reveals severe NMJ phenotypes (D) that are not rescued by overexpression of *Gαo[Q205L]* (E), *Gαo* (F) or *RNAi-sgg* (G). (H) Bouton density in *Ank2* null phenotypes. Data are shown as bouton number per length of NMJ, as percentage of control; n.s., not significant (P>0.05). (I) High magnification of *RNAi-Ank2* shows morphological defects similar to downregulation of Wg, Fz2 or Gαo. (J,K) Overexpression of Wg or Fz2 fails to rescue the reduced bouton formation (J; data shown as in Fig. 2A) and morphological abnormalities (K) of *RNAi-Ank2*. (K) Immunostaining for Dlg provides a postsynaptic marker, whereas Fz2-GFP marks the presynapse. Elongated tube-like, bouton-less staining is visible (arrow). (L) Model of microtubule cytoskeleton regulation during NMJ formation. The Wg-Fz2 ligand-receptor complex activates the heterotrimeric Go protein, releasing Gαo, which in turn inhibits the Sgg-containing destruction complex. As a result, Sgg-mediated phosphorylation of Futsch is decreased. Futsch, in parallel, interacts with Ank2, the latter additionally being under direct control by Gαo. This combined action on microtubule-binding proteins coordinately regulates the microtubule cytoskeleton, as required for synaptic remodeling. Scale bars: 10 µm in D,K; 5 µm in I.

localization of Wg-Fz2-Gαo signaling components. Altogether, Ank2 appears to act downstream of the Wg-Fz2-Gαo pathway.

As Ank2 has been shown to regulate bouton stability (Hortsch et al., 2002; Koch et al., 2008; Pielage et al., 2008), we next analyzed the extent of synaptic retractions in *Ank2* mutants with or without activation of Gαo. Loss of the microtubule-binding protein Futsch is considered as the first step of synaptic retraction, followed by loss of cytoplasmic proteins such as Synapsin (Pielage et al., 2008). In accordance with previous studies (Koch et al., 2008; Pielage et al., 2008), we observed that ~40% of the $Ank2^{-/-}$ boutons lost Synapsin staining and ~60% lost Futsch (supplementary material Fig. S3D,F,H). As expected, expression of *Gαo[Q205L]* in the $Ank2^{-/-}$ NMJs failed to restore synaptic stability when evaluated at the level of Synapsin or Futsch (supplementary material Fig. S3E,G,H). Thus, Gαo cannot rescue synapse stability in the absence of Ank2, confirming that Ank2 is epistatic to the Wg-Fz2-Gαo pathway.

We next analyzed presynaptic abnormalities in NMJs with reduced Gαo and found that ~8% of *Gαo* mutant boutons and 5.4% of the *RNAi-Gαo* boutons are completely devoid of Ank2 immunostaining [supplementary material Fig. S3I; 7.91±2.71% (n=18) and 5.41±1.73% (n=23), respectively, as compared with 0.73±0.30% (n=31) in wild-type NMJs (mean±s.e.m.); P=0.0012 and P=0.0033, respectively]. Reciprocally, in the absence of Ank2, overactivation of Gαo induces a significant number of ghost boutons and neuronal processes [bouton-like structures and interconnecting processes containing presynaptic HRP staining but lacking postsynaptic CD8-GFP-Sh (Ataman et al., 2006)] (supplementary material Fig. S3J,K); such structures are rarely visible in other genotypes (Ataman et al., 2006). Thus, it can be suggested that the Wg-Fz2-Gαo pathway recruits Ank2 to build a synapse, and in the absence of the latter the synapse does not form properly.

Gαo-ankyrin interaction is conserved in the mammalian neurite outgrowth pathway

As an independent means of proving the mechanistic relationship between Gαo and ankyrins, and to show that this interaction is of

Development (2014) 141, 3399-3409 doi:10.1242/dev.106773

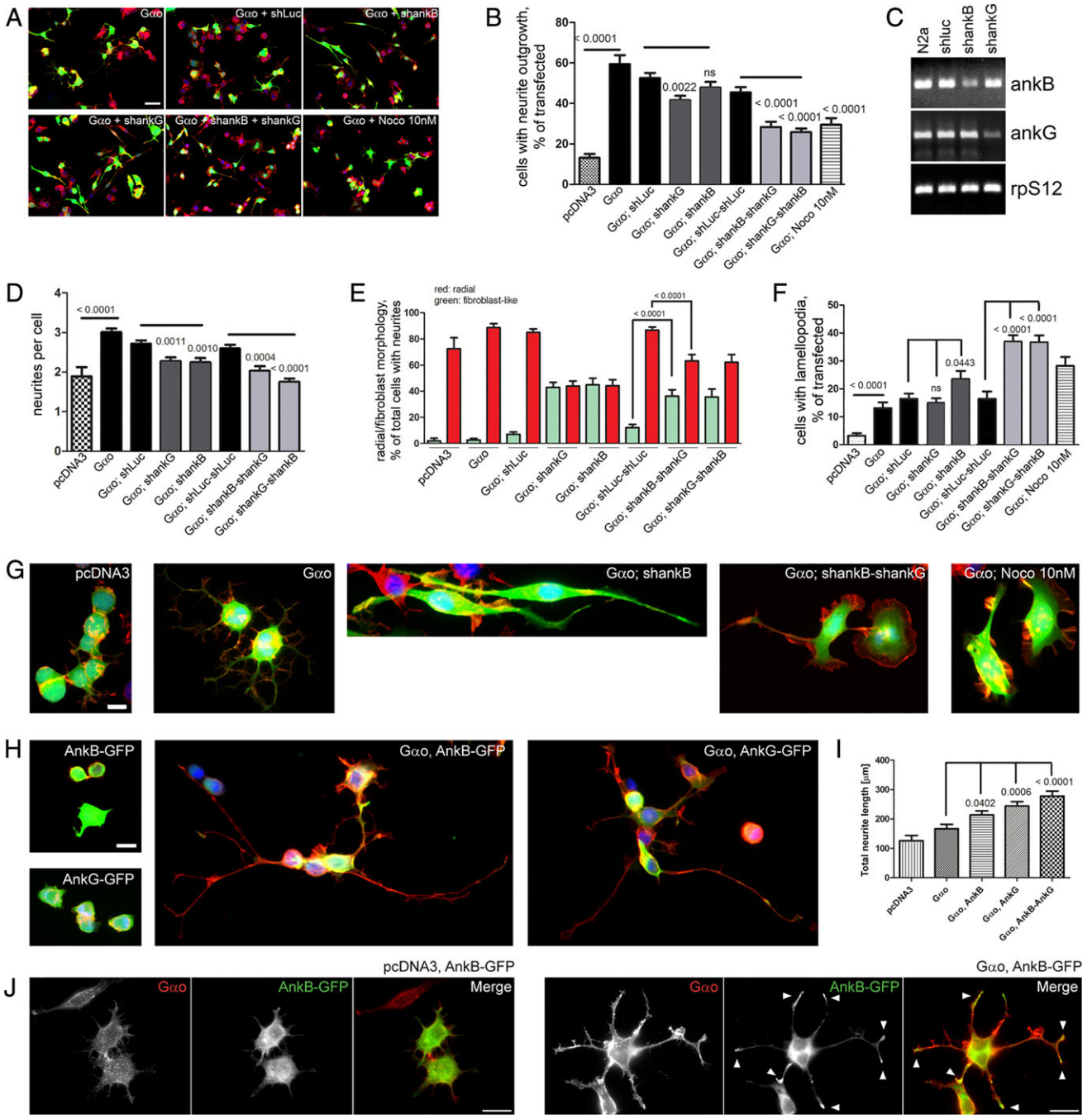

Fig. 6. Gαo-mediated neurite outgrowth and neuronal morphology in N2a cells require AnkB and AnkG. (A) Overexpression of Gαo stimulates the formation of neurites in parental mouse N2a cells and in cells stably transfected with control shRNA (shluc). Permanent shRNA-induced downregulation of *AnkB* (shankB) or *AnkG* (shankG) results in the formation of elongated fibroblast-like cells, increases lamellopodia formation and slightly reduces the percentage of cells growing neurites and the number of neurites per cell. Transient ankyrin double knockdowns achieved by transfection of the shankB and shankG stable cell lines with the shankG and shankB plasmids, respectively, strongly increase the effects observed in single knockdowns. Treatment of Gαo-overexpressing N2a cells with Nocodazole (Noco) mimics the ankyrin double-knockdown phenotypes. Co-expression of EGFP (green) marks transfected cells and staining with phalloidin-Rhodamine (red) and DAPI (blue) is used to visualize F-actin and nuclei, respectively. (B) Quantification of the effects of Gαo overexpression on neurite outgrowth as compared with control transfected (pcDNA3) N2a cells, in shRNA stably transfected cell lines and in the presence of 10 nM Nocodazole. Data represent mean±s.e.m.; horizontal black lines indicate groups of statistical analysis and *P*-values are given above each bar (ns, not significant). (C) RT-PCR analysis shows the reduction in *AnkB* and *AnkG* expression in shRNA stably transfected N2a cells. Expression of the ribosomal protein S12 gene (*Rps12*) served as control. (D-F) Quantification of effects on the number of neurites per cell (D), cell morphology (E) and lamellopodia formation (F) of overexpression of Gαo in parental and shRNA-treated N2a cells. Data representation and statistical analysis are as in B. (G) Representative images of control transfected (pcDNA3) N2a cells and Gαo overexpression in parental as well as in single and double AnkB and AnkG knockdowns. Nocodazole treatment mimics the effects of Gαo overexpression in ankyrin double knockdowns. (H) Representative images of N2a cells overexpressing EGFP-tagged AnkB or AnkG show a substantial increase in the length of neurites upon co-expression with *Gαo*, but not alone. Fluorescence as in A. (I) Quantification of total neurite length in H. Data representation and statistical analysis are as in B. (J) Overexpression of *Gαo* induced the local accumulation of AnkB-GFP at neurite tips (arrowheads), which is not observed in control cells transfected with AnkB-GFP alone. Red fluorescence indicates Gαo immunostaining. Scale bars: 20 µm in A; 10 µm in G,H,J.

Development (2014) 141, 3399-3409 doi:10.1242/dev.106773

importance beyond the *Drosophila* NMJ, we turned to the well-characterized neurite outgrowth pathway in mouse neuroblastoma N2a cells.

As previously reported (Jordan et al., 2005), we find that overexpression of *Gαo* induces strong neurite outgrowth in N2a cells (Fig. 6A,B), with ∼60% of cells forming neurites. N2a cells express both neuronal mammalian ankyrins: *AnkB* and *AnkG* (*Ank2* and *Ank3* – Mouse Genome Informatics) (Fig. 6C) (Santuccione et al., 2013). We downregulated *AnkB*, *AnkG* or both using shRNA constructs (Fig. 6C), and investigated whether Gαo was still capable of inducing neurite outgrowth in these mutant backgrounds. The overall number of N2a cells with neurite outgrowth, as well as the number of neurites per cell induced by Gαo, were decreased in *AnkB* and *AnkG* single knockdowns, and further decreased in double knockdowns (Fig. 6A,B,D).

However, the most dramatic effect of *AnkB*/*G* knockdown on Gαo-induced neurite outgrowth was seen at the level of overall cell morphology (Fig. 6E-G). Whereas *Gαo*-overexpressing cells (as well as N2a cells spontaneously producing neurites) possessed a radial morphology, with several neurites undergoing outgrowth in multiple directions (Fig. 6E,G), *Gαo* overexpression in *AnkB* and *AnkG* single knockdowns induced a very characteristic bilateral, fibroblast-like morphology (Fig. 6E,G), which often additionally included the formation of lamellopodia (Fig. 6G). Remarkably, the double knockdowns further increased the number of cells that were massively producing lamellopodia instead of neurites (Fig. 6F,G). It appears that the lamellopodial phenotype of *Gαo*-overexpressing, *AnkB*/*G* double-knockdown cells is a more severe manifestation of the fibroblast-like morphology seen in *Gαo*-overexpressing, *AnkB* or *AnkG* single-knockdown cells (Fig. 6E,F). By contrast, *AnkB*/*G* knockdowns in control cells do not change in cellular appearance (supplementary material Fig. S4A). As an independent means to induce neurite outgrowth, we overexpressed MARK2 (also known as PAR1b) (Biernat et al., 2002) and found that the resulting phenotype was unaffected by the double knockdown of *AnkB* and *AnkG* (supplementary material Fig. S4B,C), indicating that akyrins are specifically required for the Gαo-mediated neurite outgrowth pathway.

Thus, reduction in ankyrin levels dramatically alters the ability of Gαo to induce neurite outgrowth in neuronal cells and further changes the cytoskeletal response to Gαo – from neurite production to lamellopodial protrusion. We hypothesized that, in the absence of AnkB/G, the Gαo-responsive cellular program switches from the regulation of microtubules to the actin cytoskeleton. To test this, we treated the *Gαo*-overexpressing cells with different concentrations of nocodazole, which is a microtubule-depolymerizing agent known to impair neurite outgrowth (Heidemann et al., 1985). Remarkably, low nocodazole concentrations could mimic the effect of *AnkB*/*G* double knockdown in *Gαo*-overexpressing cells: the ability of Gαo to induce neurite outgrowth was reduced, with a concomitant increase in the number of lamellopodial cells (Fig. 6F,G; supplementary material Fig. S4D,E).

Next, we examined the effects of co-overexpression of *Gαo* with EGFP-tagged *AnkB* and/or *AnkG*. Notably, co-overexpression of *Gαo* and *AnkB*, *AnkG* or both induced a substantial increase in the total neurite length compared with *Gαo* overexpression alone (Fig. 6H,I), whereas the number of cells displaying neurites and the number of neurites per cell were unaffected (supplementary material Fig. S4F,G). As overexpression of *AnkB* and/or *AnkG* did not induce neurite outgrowth (Fig. 6H), these data further support the functional relationship between Gαo and ankyrins. Interestingly, AnkB (but not AnkG) significantly accumulates at the tips of neurites in *Gαo*-overexpressing cells, but not at spontaneously formed neurites in control N2a cells or at neurites induced by MARK2 co-expression (Fig. 6J; supplementary material Fig. S4H-J). These results indicate that Gαo activity is required to recruit AnkB to the growing neurite tips.

We conclude that the Gαo-Ank interaction is conserved from *Drosophila* to mammalian cells, and that this interaction is crucial for the ability of Gαo to regulate the neuronal microtubule cytoskeleton.

DISCUSSION

Synaptic plasticity underlies learning and memory. Both in invertebrates and vertebrates, activation of Wnt signaling is involved in several aspects of synapse formation and remodeling (Budnik and Salinas, 2011), and defects in this pathway may be causative of synaptic loss and neurodegeneration (Inestrosa and Arenas, 2010). Thus, understanding the molecular mechanisms of synaptic Wnt signaling is of fundamental as well as medical importance. The *Drosophila* NMJ is a powerful model system with which to study glutamatergic synapses (Collins and DiAntonio, 2007), and the Wnt pathway has been widely identified as one of the key regulators of NMJ formation (Packard et al., 2002; Mathew et al., 2005; Miech et al., 2008; Korkut et al., 2009; Mosca and Schwarz, 2010).

Here, we provide important mechanistic insights into Wnt signal transduction in the NMJ, identifying the heterotrimeric Go protein as a crucial downstream transducer of the Wg-Fz2 pathway in the presynapse. We further demonstrate that Ank2, a known player in the NMJ (Koch et al., 2008; Pielage et al., 2008), is a target of Gαo in this signaling.

We find that the α subunit of Go is strongly expressed in the presynaptic cell, and that under- or overactivation of this G protein leads to neurotransmission and behavioral defects. At the level of NMJ morphology, we find that presynaptic downregulation or Ptx-mediated inactivation of *Gαo* recapitulates the phenotypes obtained by similar silencing of *wg* and *fz2*. These data confirm that presynaptic Wg signaling, in addition to the Wg pathway active in the muscle (Mathew et al., 2005; Mosca and Schwarz, 2010), is crucial for proper NMJ formation (Miech et al., 2008), and that Go is required for this process. Furthermore, neuronal Gαo overexpression can rescue the *wg* and *fz2* loss-of-function phenotypes, demonstrating that, as in other contexts of Wnt/Fz signaling (Katanaev et al., 2005; Katanaev and Tomlinson, 2006a; Purvanov et al., 2010), Go acts as a transducer of Wg/Fz2 in NMJ formation. In contrast to its evident function and clear localization in the presynapse, Gαo localization on the muscle side of the synapse is much less pronounced or absent. Unlike Gαo, the main *Drosophila* Gβ subunit is strongly expressed in both the pre- and postsynapse. Thus, a heterotrimeric G protein other than Go might be involved in the postsynaptic Fz2 transduction, as has been implicated in Fz signaling in some other contexts (Egger-Adam and Katanaev, 2008; Koval and Katanaev, 2011; von Maltzahn et al., 2012; Nichols et al., 2013).

A recent study proposed a role for Gαo downstream of the octopamine receptor Octβ1R (Koon and Budnik, 2012). This signaling was proposed to regulate the acute behavioral response to starvation both on type II NMJs (octapaminergic) and on the type I NMJs (glutamatergic) studied here. In contrast to our observations, downregulation of Gαo in these NMJs was proposed to increase, rather than decrease, type I bouton numbers (Koon and Budnik, 2012). We suspect that the main reason for the discrepancy lies in the Gal4 lines used. The *BG439-Gal4* and *C380-Gal4* lines of Koon and Budnik are poorly characterized and, unlike the well-analyzed

Development (2014) 141, 3399-3409 doi:10.1242/dev.106773

pan-neuronal *elav-Gal4* (Luo et al., 1994) and motoneuron-specific *OK371-Gal4* (Mahr and Aberle, 2006) and *D42-Gal4* (Parkes et al., 1998) driver lines used in our study, might mediate a more acute expression. In this case, our study reflects the positive role of Gαo in the developmental formation of glutamatergic boutons, as opposed to a role in acute fine-tuning in response to environmental factors as studied by Koon and Budnik (2012).

Postsynaptic expression of *fz2* was found to fully rescue *fz2* null NMJs (Mathew et al., 2005) (supplementary material Fig. S1Q). Here, we find that presynaptic knockdown of Fz2 (and other components of Wg-Fz2-Gαo signaling) recapitulates *fz2* null phenotypes, whereas presynaptic overactivation of this pathway increases bouton numbers; furthermore, presynaptic overexpression of *fz2* or *Gαo* rescues the *fz2* nulls, just as postsynaptic overexpression of *fz2* does. Our data thus support a crucial role for presynaptic Wg-Fz2-Gαo signaling in NMJ formation. Interestingly, both pre- and postsynaptic re-introduction of Arrow, an Fz2 co-receptor that is normally present both pre- and postsynaptically, as is Fz2 itself, can rescue *arrow* mutant NMJs (Miech et al., 2008). Thus, it appears that the pre- and postsynaptic branches of Fz2 signaling are both involved in NMJ development. A certain degree of redundancy between these branches must exist. Indeed, wild-type levels of Fz2 in the muscle are not sufficient to rescue the bouton defects induced by presynaptic expression of *RNAi-fz2* (Fig. 2A,B,G), yet overexpression of *fz2* in the muscle can restore the bouton integrity of *fz2* nulls (supplementary material Fig. S1Q) (Mathew et al., 2005). One might hypothesize that postsynaptic Fz2 overexpression activates a compensatory pathway – such as that mediated by reduction in laminin A signaling (Tsai et al., 2012) – that leads to restoration in bouton numbers in *fz2* mutants. Our data showing that the targeted downregulation of Fz2 in the presynapse is sufficient to recapitulate the *fz2* null phenotype underpin the crucial function of presynaptic Fz2 signaling in NMJ formation.

We find that downregulation of *Ank2* produces NMJ defects similar to those of *wg*, *fz2* or *Gαo* silencing. However, *Ank2* mutant phenotypes appear more pronounced, indicating that Wg-Fz2-Gαo signaling might control a subset of Ank2-mediated activities in the NMJ. Ank2 was proposed to play a structural role in NMJ formation, binding to microtubules through its C-terminal region (Pielage et al., 2008). However, since the C-terminal region was insufficient to rescue *Ank2L* mutant phenotypes (Pielage et al., 2008), additional domains are likely to mediate Ank2 function through binding to other proteins. We demonstrate here in the yeast two-hybrid system and in pull-down experiments that the ankyrin repeat region of Ank2 physically binds Gαo, suggesting that the function of Ank2 in NMJ formation might be regulated by Wg-Fz2-Gαo signaling. Indeed, epistasis experiments place Ank2 downstream of Gαo in NMJ formation.

Upon dissociation of the heterotrimeric Go protein by activated GPCRs such as Fz2, the liberated Gαo subunit can signal to its downstream targets both in the GTP- and GDP-bound state (the latter after hydrolysis of GTP and before re-association with Gβγ) (Katanaev, 2010). The free signaling Gαo-GDP form is predicted to be relatively long lived (Katanaev and Chornomorets, 2007), and a number of Gαo target proteins have been identified that interact equally well with both of the nucleotide forms of this G protein (Kopein and Katanaev, 2009; Egger-Adam and Katanaev, 2010; Purvanov et al., 2010; Lin and Katanaev, 2013; Lin et al., 2014). In the context of NMJ formation, we find that Gαo-GTP and -GDP are efficient in the activation of downstream signaling, and identify Ank2 as a binding partner of Gαo that interacts with both nucleotide forms. The importance of signaling by Gα-GDP released from a heterotrimeric complex by the action of GPCRs has also been demonstrated in recent studies of mammalian chemotaxis, planar cell polarity and cancer (Ezan et al., 2013; Kamakura et al., 2013; Lin et al., 2014).

Gαo[G203T], which largely resides in the GDP-binding state owing to its reduced affinity for GTP, might be expected to act as a dominant-negative. However, in canonical Wnt signaling, regulation of asymmetric cell division as well as in planar cell polarity (PCP) signaling in the wing, Gαo[G203T] displays no dominant-negative activity but is simply silent (Katanaev et al., 2005; Katanaev and Tomlinson, 2006a), whereas in eye PCP signaling this form acts positively but is weaker than other Gαo forms (V.L.K. and A. Tomlinson, unpublished observations). Biochemical characterization of the mammalian Gαi2[G203T] mutant revealed that it can still bind Gβγ and GTP, but upon nucleotide exchange Gαi2[G203T] fails to adopt the activated confirmation and can further lose GTP (Inoue et al., 1995). Our biochemical characterization confirms that Gαo[G203T] still binds GTP (supplementary material Fig. S2C). Interestingly, Gαi2 [G203T] inhibited only a fraction of Gαi2-mediated signaling (Winitz et al., 1994), suggesting that the dominant-negative effects of the mutant are effector specific. Thus, we infer that a portion of Gαo[G203T] can form a competent Fz2-transducing complex, and a portion of overexpressed Gαo[G203T] resides in a free GDP-loaded form that is also competent to activate downstream targets – Ank2 in the context of NMJ formation.

Our experiments place Ank2 downstream of Gαo and also of Sgg (GSK3β). It remains to be investigated whether Ank2 can directly interact with and/or be phosphorylated by Sgg. Meanwhile, we propose that the microtubule-binding protein Futsch might be a linker between Sgg and Ank2. Futsch is involved in NMJ formation and is placed downstream of Wg-Sgg signaling, being the target of phosphorylation and negative regulation by Sgg as the alternative target to β-catenin, which is dispensable in Wg NMJ signaling (Hummel et al., 2000; Roos et al., 2000; Franco et al., 2004; Gogel et al., 2006; Miech et al., 2008). Abnormal Futsch localization has been observed in *Ank2* mutants (Pielage et al., 2008). In *Drosophila* wing and mammalian cells in culture, Gαo acts upstream of Sgg/GSK3β (Katanaev et al., 2005; Liu et al., 2005). Cumulatively, these data might suggest that the Wg-Fz2-Gαo cascade sends a signal to Futsch through Sgg, parallel to that mediated by Ank2 (Fig. 5L).

The importance of the Gαo-Ank2 interaction for *Drosophila* NMJ development is corroborated by our findings in mammalian neuronal cells, where we demonstrate that the ability of Gαo to induce neurite outgrowth is critically dependent on AnkB and AnkG. Knockdown of either or both ankyrin reduces neurite production. Remarkably, upon AnkB/G downregulation, Gαo switches its activity from the induction of microtubule-dependent processes (neurites) to actin-dependent protrusions (lamellopodia). Furthermore, Gαo recruits AnkB to the growing neurite tips. These data demonstrate that the Gαo-ankyrin mechanistic interactions are conserved from insects to mammals and are important for control over the neuronal tubulin cytoskeleton in the context of neurite growth and synapse formation. The novel signaling mechanism that we have uncovered (Fig. 5L) might thus be of general applicability in animal nervous system development and function.

MATERIALS AND METHODS

Fly stocks

Fly lines are described in supplementary material Methods. Fly crosses were performed at 25°C.

Development (2014) 141, 3399-3409 doi:10.1242/dev.106773

Immunostaining and microscopy analysis of NMJs

Wandering third instar larvae were dissected in PBS as described (Brent et al., 2009) before fixation and immunostaining using the antibodies described in supplementary material Methods. NMJs of muscle 6/7 in segment 2-4 were analyzed in all experiments. Maximally, two segments per animal were analyzed. NMJs were imaged with a Zeiss LSM 510 or LSM710 confocal microscope. For further details see supplementary material Methods.

Electrophysiology and muscle contraction

ChR2-mediated stimulation of synaptic potentials was performed as described (Schroll et al., 2006; Hornstein et al., 2009) and intracellular potentials were recorded in body wall muscles 6/7 (for details see supplementary material Methods).

Yeast two-hybrid screen, pull-down assay and GTP-binding assay

The yeast two-hybrid screen, biological significance score and analysis of the Gαo-interacting region in Ank2 were performed as described (Formstecher et al., 2005; Kopein and Katanaev, 2009). The first 12 ankyrin repeats of Ank2 (Ank2_12) were cloned into pMAL-c2x (New England BioLabs). The MBP-tagged Ank2_12 and MBP alone were bacterially expressed and purified. Recombinant *Drosophila* His_6-Gαo and His_6-Gαo[G203T] were purified in parallel and pull-downs and GTP-binding assays were performed as previously described (Kopein and Katanaev, 2009; Koval et al., 2010). Further details are provided in supplementary material Methods.

Mouse cell culture and neurite outgrowth assay

Mouse neuroblastoma N2a cells were cultured in MEM supplemented with 10% FCS, L-glutamine and penicillin/streptomycin (all from Gibco, Life Technologies). Vector transfections were carried out with X-tremeGENE 9 (Roche) according to the manufacturer's instructions. Permanent AnkB or AnkG depletion in N2a cells was achieved using the pRetroSuper vector (Oligoengine). For the analysis of neurite outgrowth, cells were transfected for 24 h, trypsinized and seeded on poly-L-lysine-coated coverslips for an additional 24 h to allow neurite formation. For Nocodazole (Sigma-Aldrich) treatment, transfected N2a cells were allowed to adhere on coverslips for 6 h before incubation for an additional 18 h with Nocodazole. Cells were finally fixed with 4% paraformaldehyde, stained with phalloidin-Rhodamine (Molecular Probes, Life Technologies) and DAPI (Sigma-Aldrich) or anti-Gαo antibody and mounted for microscopy analysis. For further details see supplementary material Methods.

Statistical analysis

Statistical analysis was performed with SAS JMP 7 and GraphPad Prism 5. Data are presented as mean±s.e.m. *P*-values were obtained by Student's *t*-test.

Acknowledgements

We thank Hermann Aberle, Vivian Budnik, Susan Cumberledge, Corey Goodman, Jean-Paul Vincent, Juergen Knoblich, Andrew Tomlinson, Vann Bennett, Clare Waterman, Bloomington Stock Center, Vienna *Drosophila* RNAi Stock Center, Developmental Studies Hybridoma Bank, and *Drosophila* Genomics Resource Center for generously providing fly stocks, antibodies and plasmids. We thank C. Giovanni Galizia, Claudia Stuermer and Andrew Tomlinson for critically reading the manuscript.

Competing interests

The authors declare no competing financial interests.

Author contributions

A.-M.L. performed the majority of the experiments and wrote the manuscript. G.P.S. designed and performed experiments of Fig. 6 and supplementary material Fig. S4. D.E.-A. participated in the early parts of the project. A.K. performed experiments for supplementary material Fig. S2C. C.L. produced antibodies to Gαo. M.G.B. and S.K. provided the experimental setup and consultation for electrophysiological measurements. V.L.K. designed and supervised the study, analyzed the data and wrote the manuscript.

Funding

This work was supported by grants from the Deutsche Forschungsgemeinschaft, Swiss National Science Foundation, and Synapsis Foundation to V.L.K. Deposited in PMC for immediate release.

Supplementary material

Supplementary material available online at
http://dev.biologists.org/lookup/suppl/doi:10.1242/dev.106773/-/DC1

References

Ataman, B., Ashley, J., Gorczyca, D., Gorczyca, M., Mathew, D., Wichmann, C., Sigrist, S. J. and Budnik, V. (2006). Nuclear trafficking of Drosophila Frizzled-2 during synapse development requires the PDZ protein dGRIP. *Proc. Natl. Acad. Sci. USA* **103**, 7841-7846.

Bennett, V. and Baines, A. J. (2001). Spectrin and ankyrin-based pathways: metazoan inventions for integrating cells into tissues. *Physiol. Rev.* **81**, 1353-1392.

Biernat, J., Wu, Y.-Z., Timm, T., Zheng-Fischhöfer, Q., Mandelkow, E., Meijer, L. and Mandelkow, E.-M. (2002). Protein kinase MARK/PAR-1 is required for neurite outgrowth and establishment of neuronal polarity. *Mol. Biol. Cell* **13**, 4013-4028.

Bouley, M., Tian, M. Z., Paisley, K., Shen, Y. C., Malhotra, J. D. and Hortsch, M. (2000). The L1-type cell adhesion molecule neuroglian influences the stability of neural ankyrin in the Drosophila embryo but not its axonal localization. *J. Neurosci.* **20**, 4515-4523.

Brent, J. R., Werner, K. M. and McCabe, B. D. (2009). Drosophila larval NMJ dissection. *J. Vis. Exp.* pii: 1107, doi: 10.3791/1107.

Budnik, V. and Salinas, P. C. (2011). Wnt signaling during synaptic development and plasticity. *Curr. Opin. Neurobiol.* **21**, 151-159.

Collins, C. A. and DiAntonio, A. (2007). Synaptic development: insights from Drosophila. *Curr. Opin. Neurobiol.* **17**, 35-42.

Dubreuil, R. R. and Yu, J. (1994). Ankyrin and beta-spectrin accumulate independently of alpha-spectrin in Drosophila. *Proc. Natl. Acad. Sci. USA* **91**, 10285-10289.

Egger-Adam, D. and Katanaev, V. L. (2008). Trimeric G protein-dependent signaling by Frizzled receptors in animal development. *Front. Biosci.* **13**, 4740-4755.

Egger-Adam, D. and Katanaev, V. L. (2010). The trimeric G protein Go inflicts a double impact on axin in the Wnt/frizzled signaling pathway. *Dev. Dyn.* **239**, 168-183.

Ezan, J., Lasvaux, L., Gezer, A., Novakovic, A., May-Simera, H., Belotti, E., Lhoumeau, A.-C., Birnbaumer, L., Beer-Hammer, S., Borg, J.-P. et al. (2013). Primary cilium migration depends on G-protein signalling control of subapical cytoskeleton. *Nat. Cell Biol.* **15**, 1107-1115.

Formstecher, E., Aresta, S., Collura, V., Hamburger, A., Meil, A., Trehin, A., Reverdy, C., Betin, V., Maire, S., Brun, C. et al. (2005). Protein interaction mapping: a Drosophila case study. *Genome Res.* **15**, 376-384.

Franco, B., Bogdanik, L., Bobinnec, Y., Debec, A., Bockaert, J., Parmentier, M.-L. and Grau, Y. (2004). Shaggy, the homolog of glycogen synthase kinase 3, controls neuromuscular junction growth in Drosophila. *J. Neurosci.* **24**, 6573-6577.

Gilman, A. G. (1987). G proteins: transducers of receptor-generated signals. *Annu. Rev. Biochem.* **56**, 615-649.

Gögel, S., Wakefield, S., Tear, G., Klämbt, C. and Gordon-Weeks, P. R. (2006). The Drosophila microtubule associated protein Futsch is phosphorylated by Shaggy/Zeste-white 3 at an homologous GSK3beta phosphorylation site in MAP1B. *Mol. Cell. Neurosci.* **33**, 188-199.

Guan, B., Hartmann, B., Kho, Y.-H., Gorczyca, M. and Budnik, V. (1996). The Drosophila tumor suppressor gene, dlg, is involved in structural plasticity at a glutamatergic synapse. *Curr. Biol.* **6**, 695-706.

Heidemann, S. R., Joshi, H. C., Schechter, A., Fletcher, J. R. and Bothwell, M. (1985). Synergistic effects of cyclic AMP and nerve growth factor on neurite outgrowth and microtubule stability of PC12 cells. *J. Cell Biol.* **100**, 916-927.

Hornstein, N. J., Pulver, S. R. and Griffith, L. C. (2009). Channelrhodopsin2 mediated stimulation of synaptic potentials at Drosophila neuromuscular junctions. *J. Vis. Exp.* e1133.

Hortsch, M., Paisley, K. L., Tian, M.-Z., Qian, M., Bouley, M. and Chandler, R. (2002). The axonal localization of large Drosophila ankyrin2 protein isoforms is essential for neuronal functionality. *Mol. Cell. Neurosci.* **20**, 43-55.

Hummel, T., Krukkert, K., Roos, J., Davis, G. and Klämbt, C. (2000). Drosophila Futsch/22C10 is a MAP1B-like protein required for dendritic and axonal development. *Neuron* **26**, 357-370.

Inestrosa, N. C. and Arenas, E. (2010). Emerging roles of Wnts in the adult nervous system. *Nat. Rev. Neurosci.* **11**, 77-86.

Inoue, S., Hoshino, S., Kukimoto, I., Ui, M. and Katada, T. (1995). Purification and characterization of the G203T mutant alpha i-2 subunit of GTP-binding protein expressed in baculovirus-infected Sf9 cells. *J. Biochem.* **118**, 650-657.

Jan, L. Y. and Jan, Y. N. (1982). Antibodies to horseradish peroxidase as specific neuronal markers in Drosophila and in grasshopper embryos. *Proc. Natl. Acad. Sci. USA* **79**, 2700-2704.
Jordan, J. D., He, J. C., Eungdamrong, N. J., Gomes, I., Ali, W., Nguyen, T., Bivona, T. G., Philips, M. R., Devi, L. A. and Iyengar, R. (2005). Cannabinoid receptor-induced neurite outgrowth is mediated by Rap1 activation through G (alpha)o/i-triggered proteasomal degradation of Rap1GAPII. *J. Biol. Chem.* **280**, 11413-11421.
Kamakura, S., Nomura, M., Hayase, J., Iwakiri, Y., Nishikimi, A., Takayanagi, R., Fukui, Y. and Sumimoto, H. (2013). The cell polarity protein mInsc regulates neutrophil chemotaxis via a noncanonical G protein signaling pathway. *Dev. Cell* **26**, 292-302.
Katanaev, V. L. (2010). The Wnt/Frizzled GPCR signaling pathway. *Biochemistry* **75**, 1428-1434.
Katanaev, V. L. and Chornomorets, M. (2007). Kinetic diversity in G-protein-coupled receptor signalling. *Biochem. J.* **401**, 485-495.
Katanaev, V. L. and Tomlinson, A. (2006a). Dual roles for the trimeric G protein Go in asymmetric cell division in Drosophila. *Proc. Natl. Acad. Sci. USA* **103**, 6524-6529.
Katanaev, V. L. and Tomlinson, A. (2006b). Multiple roles of a trimeric G protein in Drosophila cell polarization. *Cell Cycle* **5**, 2464-2472.
Katanaev, V. L., Ponzielli, R., Sémériva, M. and Tomlinson, A. (2005). Trimeric G protein-dependent frizzled signaling in Drosophila. *Cell* **120**, 111-122.
Katanayeva, N., Kopein, D., Portmann, R., Hess, D. and Katanaev, V. L. (2010). Competing activities of heterotrimeric G proteins in Drosophila wing maturation. *PLoS ONE* **5**, e12331.
Koch, I., Schwarz, H., Beuchle, D., Goellner, B., Langegger, M. and Aberle, H. (2008). Drosophila ankyrin 2 is required for synaptic stability. *Neuron* **58**, 210-222.
Koon, A. C. and Budnik, V. (2012). Inhibitory control of synaptic and behavioral plasticity by octopaminergic signaling. *J. Neurosci.* **32**, 6312-6322.
Kopein, D. and Katanaev, V. L. (2009). Drosophila GoLoco-protein pins is a target of Galpha(o)-mediated G protein-coupled receptor signaling. *Mol. Biol. Cell* **20**, 3865-3877.
Korkut, C., Ataman, B., Ramachandran, P., Ashley, J., Barria, R., Gherbesi, N. and Budnik, V. (2009). Trans-synaptic transmission of vesicular Wnt signals through Evi/Wntless. *Cell* **139**, 393-404.
Koval, A. and Katanaev, V. L. (2011). Wnt3a stimulation elicits G-protein-coupled receptor properties of mammalian Frizzled proteins. *Biochem. J.* **433**, 435-440.
Koval, A., Kopein, D., Purvanov, V. and Katanaev, V. L. (2010). Europium-labeled GTP as a general nonradioactive substitute for [(35)S]GTPgammaS in high-throughput G protein studies. *Anal. Biochem.* **397**, 202-207.
Lin, C. and Katanaev, V. L. (2013). Kermit interacts with galphao, vang, and motor proteins in Drosophila planar cell polarity. *PLoS ONE* **8**, e76885.
Lin, C., Koval, A., Tishchenko, S., Gabdulkhakov, A., Tin, U., Solis, G. P. and Katanaev, V. L. (2014). Double suppression of the Galpha protein activity by RGS proteins. *Mol. Cell* **53**, 663-671.
Liu, X., Rubin, J. S. and Kimmel, A. R. (2005). Rapid, Wnt-induced changes in GSK3beta associations that regulate beta-catenin stabilization are mediated by Galpha proteins. *Curr. Biol.* **15**, 1989-1997.
Logan, C. Y. and Nusse, R. (2004). The Wnt signaling pathway in development and disease. *Annu. Rev. Cell Dev. Biol.* **20**, 781-810.
Luo, L., Liao, Y. J., Jan, L. Y. and Jan, Y. N. (1994). Distinct morphogenetic functions of similar small GTPases: Drosophila Drac1 is involved in axonal outgrowth and myoblast fusion. *Genes Dev.* **8**, 1787-1802.
Mahr, A. and Aberle, H. (2006). The expression pattern of the Drosophila vesicular glutamate transporter: a marker protein for motoneurons and glutamatergic centers in the brain. *Gene Expr. Patterns* **6**, 299-309.
Mathew, D., Ataman, B., Chen, J., Zhang, Y., Cumberledge, S. and Budnik, V. (2005). Wingless signaling at synapses is through cleavage and nuclear import of receptor DFrizzled2. *Science* **310**, 1344-1347.
Miech, C., Pauer, H.-U., He, X. and Schwarz, T. L. (2008). Presynaptic local signaling by a canonical wingless pathway regulates development of the Drosophila neuromuscular junction. *J. Neurosci.* **28**, 10875-10884.
Mosca, T. J. and Schwarz, T. L. (2010). The nuclear import of Frizzled2-C by Importins-beta11 and alpha2 promotes postsynaptic development. *Nat. Neurosci.* **13**, 935-943.
Nichols, A. S., Floyd, D. H., Bruinsma, S. P., Narzinski, K. and Baranski, T. J. (2013). Frizzled receptors signal through G proteins. *Cell. Signal.* **25**, 1468-1475.
Packard, M., Koo, E. S., Gorczyca, M., Sharpe, J., Cumberledge, S. and Budnik, V. (2002). The Drosophila Wnt, wingless, provides an essential signal for pre- and postsynaptic differentiation. *Cell* **111**, 319-330.
Parkes, T. L., Elia, A. J., Dickinson, D., Hilliker, A. J., Phillips, J. P. and Boulianne, G. L. (1998). Extension of Drosophila lifespan by overexpression of human SOD1 in motorneurons. *Nat. Genet.* **19**, 171-174.
Pielage, J., Cheng, L., Fetter, R. D., Carlton, P. M., Sedat, J. W. and Davis, G. W. (2008). A presynaptic giant ankyrin stabilizes the NMJ through regulation of presynaptic microtubules and transsynaptic cell adhesion. *Neuron* **58**, 195-209.
Purvanov, V., Koval, A. and Katanaev, V. L. (2010). A direct and functional interaction between Go and Rab5 during G protein-coupled receptor signaling. *Sci. Signal.* **3**, ra65.
Roos, J., Hummel, T., Ng, N., Klämbt, C. and Davis, G. W. (2000). Drosophila Futsch regulates synaptic microtubule organization and is necessary for synaptic growth. *Neuron* **26**, 371-382.
Santuccione, A. C., Merlini, M., Shetty, A., Tackenberg, C., Bali, J., Ferretti, M. T., McAfoose, J., Kulic, L., Bernreuther, C., Welt, T. et al. (2013). Active vaccination with ankyrin G reduces beta-amyloid pathology in APP transgenic mice. *Mol. Psychiatry* **18**, 358-368.
Schaefer, M., Petronczki, M., Dorner, D., Forte, M. and Knoblich, J. A. (2001). Heterotrimeric G proteins direct two modes of asymmetric cell division in the Drosophila nervous system. *Cell* **107**, 183-194.
Schnorrer, F., Schönbauer, C., Langer, C. C. H., Dietzl, G., Novatchkova, M., Schernhuber, K., Fellner, M., Azaryan, A., Radolf, M., Stark, A. et al. (2010). Systematic genetic analysis of muscle morphogenesis and function in Drosophila. *Nature* **464**, 287-291.
Schroll, C., Riemensperger, T., Bucher, D., Ehmer, J., Völler, T., Erbguth, K., Gerber, B., Hendel, T., Nagel, G., Buchner, E. et al. (2006). Light-induced activation of distinct modulatory neurons triggers appetitive or aversive learning in Drosophila larvae. *Curr. Biol.* **16**, 1741-1747.
Sternweis, P. C. and Robishaw, J. D. (1984). Isolation of two proteins with high affinity for guanine nucleotides from membranes of bovine brain. *J. Biol. Chem.* **259**, 13806-13813.
Tsai, P.-I., Wang, M., Kao, H.-H., Cheng, Y.-J., Lin, Y.-J., Chen, R.-H. and Chien, C.-T. (2012). Activity-dependent retrograde laminin A signaling regulates synapse growth at Drosophila neuromuscular junctions. *Proc. Natl. Acad. Sci. USA* **109**, 17699-17704.
von Maltzahn, J., Bentzinger, C. F. and Rudnicki, M. A. (2012). Wnt7a-Fzd7 signalling directly activates the Akt/mTOR anabolic growth pathway in skeletal muscle. *Nat. Cell Biol.* **14**, 186-191.
Wagh, D. A., Rasse, T. M., Asan, E., Hofbauer, A., Schwenkert, I., Dürrbeck, H., Buchner, S., Dabauvalle, M.-C., Schmidt, M., Qin, G. et al. (2006). Bruchpilot, a protein with homology to ELKS/CAST, is required for structural integrity and function of synaptic active zones in Drosophila. *Neuron* **49**, 833-844.
Winitz, S., Gupta, S. K., Qian, N. X., Heasley, L. E., Nemenoff, R. A. and Johnson, G. L. (1994). Expression of a mutant Gi2 alpha subunit inhibits ATP and thrombin stimulation of cytoplasmic phospholipase A2-mediated arachidonic acid release independent of Ca2+ and mitogen-activated protein kinase regulation. *J. Biol. Chem.* **269**, 1889-1895.
Wolfgang, W. J., Quan, F., Goldsmith, P., Unson, C., Spiegel, A. and Forte, M. (1990). Immunolocalization of G protein alpha-subunits in the Drosophila CNS. *J. Neurosci.* **10**, 1014-1024.
Zito, K., Parnas, D., Fetter, R. D., Isacoff, E. Y. and Goodman, C. S. (1999). Watching a synapse grow: noninvasive confocal imaging of synaptic growth in Drosophila. *Neuron* **22**, 719-729.

SUPPLEMENTARY METHODS

Fly stocks

The following lines used were: *OK371-Gal4* (Mahr and Aberle, 2006); *CD8-GFP-Sh* (Zito et al., 1999); *UAS-RNAi-ank2L* (Pielage et al., 2008); *UAS-GFP-Wg* (Pfeiffer et al., 2002); *UAS-Ptx*, *UAS-Gαo*, *UAS-Gαo[Q205L]*, *UAS-Gαo[G203T]* (Katanaev et al., 2005); *UAS-Fz2* (Chen et al., 2004); *UAS-Fz* (Strapps and Tomlinson, 2001); *UAS-wg-GFP* (Pfeiffer et al., 2002); *omb-Gal4* (Lecuit et al., 1996). The following lines were from the Vienna *Drosophila* RNAi Center (Dietzl et al., 2007): *UAS-RNAi-fz2* (VDRC#44391), *UAS-RNAi-Gαo* (#19124 and #110552 were used with identical results), *UAS-RNAi-wg* (#13351), *UAS-RNAi-ank2* (#26121), *UAS-RNAi-sgg* (#7005). *Df(3L)ED4782* deficiency (Hummel et al., 2000), *UAS-ChR2* (Schroll et al., 2006), *elav-Gal4*, D42-Gal4, *BG487-Gal4*, *GMR-Gal4* and *UAS-myr-mRFP* were from the Bloomington Stock Center. The *fz2* mutant condition was $fz2^{C1}$/ *Df(3L)ED4782* following Mathew et al. (2005). The $ank2^{E380}$ and $ank2^{K327}$ alleles (Koch et al., 2008) were used in the transheterozygote combination to analyze the *Ank2* mutant phenotypes. Although *Gαo* mutant alleles are embryonic lethal (Fremion et al., 1999; Katanaev et al., 2005), we could obtain third instar larvae of the transheterozygous genotype $Gαo^{007}$/$Gαo^{EXGO-UK}$. The first allele is a hypomorph (Fremion et al., 1999), whereas the second is a small deletion in the region (gift from A. Tomlinson). The transheterozygous larvae emerged from the genetic cross at a frequency of 23% (expected frequency 33%) but developed 1-2 days later than their heterozygous siblings; they died during early pupal stages. For the *Gαo* rescue experiments, $Gαo^{EXGO-UK}$ was recombined with *OK371-Gal4*; the presence of the driver in the recombinant was confirmed by crossing to *UAS-myr-mRFP*; the presence of the mutation was confirmed by lethality over the parental and other *Gαo* alleles. The muscle size of the heterozygous larvae was somewhat reduced compared with control larvae (Fig. S2F). All crosses were performed at 25°C.

Antibodies and immunohistochemistry

Wandering third instar larvae were dissected in PBS as described (Brent et al., 2009), fixed in 3.7% formaldehyde/PBS or, in the case of anti-Wg staining, in Bouins fixative (Reactives RAL) for 15 min and washed three times in PBS for 10 min. The dissected larvae were incubated in PBS containing 0.05% Triton X-100 (PBT) + 5% normal goat serum (NGS) for at least 30 min at room temperature. Primary antibodies were diluted in PBT plus 5% NGS and incubated at room temperature for 2 h or at 4°C overnight. The following primary antibodies were used: Cy3-coupled goat anti-HRP (123-165-021, Jackson ImmunoResearch) at 1:200; rabbit anti-Wg (Reichsman et al., 1996) at 1:300; rabbit anti-Fz2 (Packard et al., 2002) at 1:10,000; rabbit anti-Gβ13F (Schaefer et al., 2001) at 1:250; and anti-Ank2XL (Koch et al., 2008) at 1:500; mouse anti-Brp (nc82), anti-Dlg (4F3), anti-Futsch (22C10) and anti-Synapsin (3C11) (all at 1:100; Developmental Studies Hybridoma Bank); rabbit anti-Gαo at 1:100 (Merck, #371726, raised against the C-terminal decapeptide of human Gαo and Gαi3). The specificity of these anti-Gαo antibodies to recognize *Drosophila* Gαo but not Gαi was confirmed in wing imaginal discs of *omb-Gal4; UAS-Gαo* and *omb-Gal4; UAS-Gαi* larvae (Fig. S1E,F). The efficiency of these overexpression lines had been tested previously (Katanaev and Tomlinson, 2006); wing discs were immunostained as described (Katanaev et al., 2005). Additionally, the specificity of these antibodies (1:1000) to *Drosophila* Gαo but not Gαi was proven by western blots of head extracts (Kopein and Katanaev, 2009) from wild-type, *UAS-Gαo; GMR-Gal4* and *UAS-Gαi; GMR-Gal4* flies (Fig. S1G). Gαi, migrating lower than Gαo on SDS-PAGE, was undetected in *Drosophila* heads without overexpression, but was efficiently overexpressed with the *UAS-Gαi* construct as detected by polyclonal anti-Gαi antibodies (Merck, #371723, raised against the C-terminal decapeptide of human Gαi1 and Gαi2; used at 1:1000); these antibodies also recognized *Drosophila* Gαo (Fig. S1G). Additional rabbit polyclonal antibodies against *Drosophila* Gαo

were raised using the recombinant protein purified from bacteria (Kopein and Katanaev, 2009); the antiserum was used at 1:100 for immunostaining. Specificity of this antiserum was confirmed by western blots on *Drosophila* head extracts, as well as by immunostaining of wing imaginal discs. Secondary antibodies were HRP labeled for western blots (1:4000) or Cy3- and Cy5-labeled in immunostaining (1:400 in PBT, 2h incubation at room temperature). The preparations were mounted in Vectashield (Vector Labs), dorsal side up.

Microscopy and analysis of NMJs

The well-characterized NMJs of muscle 6/7 in segment 2-4 were analyzed in all experiments. Maximally, two segments per animal (e.g. segment A3 and A4, both in the same hemisphere, or both segments A3 in the two hemispheres) were analyzed. NMJs were imaged with a confocal microscope (Zeiss LSM 510 or Zeiss LSM710). For statistical analysis, one optical slice with a thickness of 2.3 µm was taken with a 20x or a 25x objective in the optical plane of each NMJ and the boutons were measured manually with the help of the program AxioVision 4.7 (Zeiss). A bouton was identified by the CD8-GFP-Sh, anti-Dlg and/or anti-HRP staining as a circular or slightly oval structure with clear borders, connected by neurites to the neighboring bouton; all these methods resulted in identical bouton quantifications. Type 1b boutons were distinguished from type Is by more intense anti-Dlg staining and their larger size (Packard et al., 2002). Bouton number values are depicted as percentage of the respective control. The length of the NMJ was measured from the first to the last bouton along the synaptic cleft and all side branches on the muscle surface with more than three boutons were measured and added to the total length of the NMJ. The lengths of the NMJ slightly varied depending on the phenotype, in agreement with (Mathew et al., 2005) (Fig. S2E).

To confirm that the *OK371-Gal4/UAS-RNAi* system was efficient to downregulate Gαo, Wg and Fz2, respective immunostainings of wild-type and *RNAi*-expressing NMJs were

performed in parallel. NMJs were imaged with a LSM710 (Zeiss) confocal microscope using identical settings for all images. Quantification of the fluorescence was performed with ImageJ (NIH). The presynaptic cell was outlined with the freehand selection tool following the borders of the staining and the mean value of the fluorescence of this area was measured with the measure tool. A noticeable downregulation in the levels of the respective proteins was achieved (Fig. S1I,M,O), and quantification revealed a ~50% decrease in anti-Gαo/Wg/Fz2 staining in the NMJ (Fig. S1J,N,P). However, this is likely to be a gross underestimation of the efficiency of the RNAi-mediated downregulation: using a pan-neuronal driver (*elav-Gal4*), we find a comparable decrease in anti-Gαo immunostaining (Fig. S1K), but in western blots on whole-head extracts of the control versus the *RNAi-Gαo* constructs, a dramatic decrease in Gαo levels could be seen (Fig. S1L). Mouse anti-tubulin (Sigma, 1:2500) staining served as loading control.

Electrophysiology and muscle contraction

ChR2-mediated stimulation of synaptic potentials was performed as described (Schroll et al., 2006; Hornstein et al., 2009). Larvae expressing ChR2 in motoneurons using the driver *OK371-Gal4* were grown on standard corn food supplemented with 1 mM *all-trans*-retinal (Sigma) at 25°C in the dark. Wandering third instar larvae were dissected in cold Ca^{2+}-free HL-3 saline (Zhang and Stewart, 2010) and washed three times in cold HL-3 supplemented with 1.5 mM $CaCl_2$ before performing the measurements in same buffer. Intracellular potentials were recorded in body wall muscles 6/7 using a pipette with a resistance of 15-30 MΩ when filled with 1 M KCl. To evoke single action potentials, animals were stimulated by a 20 ms light pulse of 470 nm using a high-power LED placed 10 cm from the larvae (light pulse triggered at 1.2V, Thorlabs) controlled by Chart Master software (HEKA). Electrophysiological signals were pre-amplified (without filtering) using the LPF-8 signal conditioner (Warner Instruments) and the 50 Hz noise was reduced using the HumBug (Quest scientific) noise reducer. Finally, analog signals were

measured using a KS-700 amplifier (World Precision Instruments) then digitized using LIH8+8 (HEKA). Data were acquired using the Chart Master software at a sampling frequency of 20 kHz. The data were low-pass filtered at 2 kHz before analysis of EJPs and mEJPs with the Mini analysis program (Synaptosoft). The threshold for detection of peaks was set to 0.3 mV. For analysis only muscles with a resting potential more negative than –46 mV were used. Note that the optogenetic measurements used here and the traditional electrophysiological recordings produce identical EJP amplitudes when measured side-by-side (Pulver et al., 2011) (note also that, in this particular work, utilizing the same *OK371-Gal4* driver as used by us, the EJP amplitude in the wild-type is measured as ~12.5 mV, very similar to our measurement of 11 mV; see Fig. 1H). Furthermore, when performing our own optogenetic measurements, we sometimes (rarely) observed non-stimulated, spontaneous action potentials which were of the same amplitude as the light-induced ones (such an example is shown on Fig. S1T).

For the locomotion test, third instar larvae were placed on a 1% agarose plate and allowed to adjust for 1 min. The number of whole body contractions per minute was counted.

Yeast two-hybrid screen

Isoform II of *Drosophila* Gαo was used as the bait, and the cDNA library from *Drosophila* head was used as the prey in the screening custom-performed by Hybrigenics (Paris, France). Fifty four million clones were screened and analyzed as described (Kopein and Katanaev, 2009). The three clones of Ank2 representing partial open reading frames each had the high confidence interaction score]biological significance score (Formstecher et al., 2005)] (B, *E*-value < 1e–5). The Gαo-interacting region in Ank2 was determined as described (Formstecher et al., 2005; Kopein and Katanaev, 2009).

Biochemistry

We amplified the first 12 ankyrin repeats of Ank2 from cDNA clone RE55168 (*Drosophila* Genomics Resource Center, EST collection) using primers 5'-GGGCATGCATGGCCCAGTTTGTGACC-3' and 5'-CCGGTACCGGCACTAATGCTGGCACC-3' and inserted the fragment into pMAL-c2x (New England Biolabs). The MBP-tagged protein was expressed in TOP10F' cells (Invitrogen). Transformed cells were grown at 37°C until OD_{600} = 0.7, cooled to 17°C before induction with 0.1 mM IPTG and subsequent growth overnight at 17°C, and then harvested by 15 min centrifugation at 4000 ***g***. The pellet was resuspended in column buffer [20 mM Tris-HCl, 200 mM NaCl, 1 mM EDTA, 1 mM DTT, 1 mg/ml lysozyme, 1x Complete protease inhibitor cocktail (Roche)] and incubated on ice for 30-60 min before sonification lysis, followed by centrifugation for 30 min at 16,000 ***g*** to remove cell debris. The protein was bound to amylose resin (New England BioLabs) by incubation at 4°C for at least 1 h. The amylose beads were washed three times for 10-15 min with column buffer and the protein was eluted with 10 mM maltose in column buffer. Control MBP was prepared using the pMAL-c2x plasmid in parallel.

The Gαo[G203T] mutation was introduced by site mutagenesis using pQE32-Gαo (Kopein and Katanaev, 2009) as the template. The following primers were used: sense, AATTGTTTGACGTGACCGGTCAGCGCTC; antisense, GAGCGCTGACCGGTCACGTCAAACAATT. Recombinant *Drosophila* His_6-Gαo was prepared and preloaded with 1 mM GDP or GTPγS as described (Kopein and Katanaev, 2009); His_6-Gαo[G203T] was purified in parallel.

Pull-down assays

Thirty micrograms of His_6-Gαo were incubated with a twofold molar excess of MBP or MBP-Ank2_12 in HKB* buffer (100 mM KCl, 50 mM HEPES-KOH, 10 mM NaCl, 5 mM $MgCl_2$, 2 mM EGTA, 1 mM DTT, 5% glycerol, 0.5% NP40, 0.1% Tween) at 17°C for 1.5 h, prior to

addition to 100 µl 50% amylose resin slurry (New England BioLabs) pre-equilibrated with HKB* for an additional 1.5 h incubation at 17°C. The resin was washed four times with 1.5 ml HKB* for 15 min. The retained proteins were eluted by a 15 min incubation with 50 µl 10 mM maltose in HKB*. The proteins were resolved on 10% SDS-PAGE, electrotransferred to nitrocellulose membranes (Whatman) and detected by immunoblotting using rabbit anti-Gαo/i at 1:1000 (Merck). Equal loading was ensured by immunoblotting using rabbit anti-MBP antibodies at 1:4000 (New England Biolabs). For experiments with Gβγ, His6-Gαo was pre-incubated with the βγ dimer purified from porcine brains (Koval et al., 2010) for 45 min at room temperature before addition of equimolar amounts of MBP-Ank2_12 or MBP and incubation for an additional 1.5 h at 4°C. The pre-equilibrated resin was added to the proteins, incubated for 1.5 h and washed as described above. Proteins were eluted by addition of 5x sample buffer and boiling.

GTP-binding assay

Poorly hydrolysable fluorescent GTP analog Eu-GTP (PerkinElmer) was used in the GTP-binding assay with purified His_6-tagged *Drosophila* Gαo and Gαo[G203T] as described (Koval et al., 2010). The indicated (Fig. S2C) concentrations of the proteins were incubated for 2 hours in the presence of 5 nM GTP-Eu in 1xHKB buffer (10 mM HEPES-NaOH, 135 mM KCl, 10 mM NaCl, 2 mM EGTA, pH 7.5) supplemented with 5 mM $MgCl_2$. The reaction mixtures were subsequently transferred to AcroWell BioTrace NT 96-well plates (Pall), filtered using a vacuum manifold, and the membranes were washed twice with ice-cold washing buffer (20 mM Tris-HCl, 0.1 mM $MgCl_2$, pH 8.0). Fluorescence of the label retained on the membranes was measured immediately in a Victor^3 multilabel counter (PerkinElmer) in TRF mode. All experimental points were measured in duplicate. Curve fitting was performed in Prism 5 software (GraphPad).

Cell culture

Mouse neuroblastoma N2a cells were cultured in MEM supplemented with 10% FCS, L-glutamine and penicillin/streptomycin (all from Gibco, Life Technologies). Vector transfections were carried out with X-tremeGENE 9 (Roche) according to the manufacturer's instructions. Permanent AnkB or AnkG depletion in N2a cells was obtained by shRNA interference using annealed primers inserted into the *Bam*HI and *Hin*dIII sites of the pRetroSuper vector. Specific target sequences for murine *AnkB* and *AnkG* were previously described (Ayalon et al., 2008). Primers used for *AnkB*: 5′ sense strand, 5′-gatccccGAGTGGCCAACATCATATAttcaagagaTATATGATGTTGGCCACTCttttta-3′; and 3′ antisense strand, 5′-agcttaaaaaGAGTGGCCAACATCATATAtctcttgaaTATATGATGTTGGCCACTCggg-3′. For *AnkG*: 5′ sense strand, 5′-gatccccGGCAGACAGACGCCAGAGCttcaagagaGCTCTGGCGTCTGTCTGCCttttta-3′; and 3′ antisense strand, 5′-agcttaaaaaGGCAGACAGACGCCAGAGCtctcttgaaGCTCTGGCGTCTGTCTGCCggg-3′. A shluc vector expressing an shRNA against firefly luciferase was used as control. To generate stable lines, shRNA vectors were transfected into N2a cells and selection was performed in normal medium supplemented with 10 μg/ml puromycin. Downregulation of *AnkB* and *AnkG* expression was confirmed by standard RT-PCR methods using primers that recognize all ankyrin isoforms: ankB-For 5′-ACAGGTGATGGGGGAGAATAC-3′; ankB-Rev 5′-GAGTCCATTGTGTCTGCATCC-3′; ankG-For 5′-GCCTGCTCATAGGAAGAGGAA-3′; ankG-Rev 5′-GTCATGACCTTGTTGCAGAGC-3′. Primers to detect expression of the ribosomal protein S12 gene were used as control: S12-For 5′-GGGGCTAGCGCCACCATGGCCGAGGAAGGCATTGC-3′; S12-Rev 5′-GGGAGATCTTCATTTCTTGCATTTGAAATAC-3′.

Neurite outgrowth assay

N2a cells were co-transfected for 24 h with pEGFP-C1 (Clontech) and pcDNA3.1+ (Invitrogen) or a plasmid encoding human Gαo (Missouri S&T cDNA Resource Center). Cells were trypsinized and seeded on poly-L-lysine-coated coverslips for an additional 24 h to allow neurite formation. Alternatively, cells were transfected with EGFP-tagged ankyrin-B or ankyrin-G vectors (Ayalon et al., 2008) or co-transfected with the Gαo plasmid and prepared as above. Transient ankyrin double knockdowns were obtained by co-transfection of the shRNA-stably transfected N2a cell lines with the shRNA vectors shluc, shankB or shankG in addition to the plasmids described above. Ankyrin-independent neurite outgrowth was analyzed using an EGFP-tagged MARK2 (PAR1b) plasmid (Nishimura et al., 2012) under the transient double ankyrin knockdown conditions described above. Additionally, an mRFP-tagged MARK2 plasmid was generated by subcloning the *Bgl*II-*Kpn*I fragment including the MARK2 sequence into the same sites of the pmRFP-C1 vector. Then, N2a cells were co-transfected with the mRFP-MARK2 and AnkB-GFP plasmids and prepared as above. AnkB-GFP mean fluorescence intensities at the rear end of neurites (10-20 μm^2) and at whole neurites were scored from 40-80 neurites per condition using ImageJ, and the ratio values were used to determine AnkB-GFP accumulation at neurite tips in cells co-transfected with control pcDNA3.1+, Gαo or mRFP-MARK2 plasmids. For Nocodazole treatment, transfected N2a cells were allowed to adhere on coverslips for 6 h before incubation for an additional 18 h with Nocodazole (Sigma-Aldrich) in normal medium at the concentrations indicated in the corresponding figures. Cells were finally fixed with paraformaldehyde, stained with phalloidin-Rhodamine (Molecular Probes, Life Technologies) and DAPI (Sigma-Aldrich) or anti-Gαo antibody and mounted for microscopy analysis. Samples were recorded with an α-Plan-Apochromat 63x/1.4 or a Plan-Neofluar 20x/0.50 objective on an

AxioImager M1 microscope equipped with an AxioCam HRc camera and analyzed using AxioVision software (all from Zeiss). The number of transfected cells displaying neurites and lamellopodia, neurites per cell, total neurite length, and cell morphology were scored from 15-20 randomly taken images (>200 cells per condition).

Supplementary references

Ayalon, G., Davis, J. Q., Scotland, P. B. and Bennett, V. (2008) 'An ankyrin-based mechanism for functional organization of dystrophin and dystroglycan', *Cell* 135(7): 1189-200.

Brent, J. R., Werner, K. M. and McCabe, B. D. (2009) 'Drosophila larval NMJ dissection', *J Vis Exp*(24).

Chen, C. M., Strapps, W., Tomlinson, A. and Struhl, G. (2004) 'Evidence that the cysteine-rich domain of Drosophila Frizzled family receptors is dispensable for transducing Wingless', *Proceedings of the National Academy of Sciences of the United States of America* 101(45): 15961-6.

Dietzl, G., Chen, D., Schnorrer, F., Su, K. C., Barinova, Y., Fellner, M., Gasser, B., Kinsey, K., Oppel, S., Scheiblauer, S. et al. (2007) 'A genome-wide transgenic RNAi library for conditional gene inactivation in Drosophila', *Nature* 448(7150): 151-6.

Formstecher, E., Aresta, S., Collura, V., Hamburger, A., Meil, A., Trehin, A., Reverdy, C., Betin, V., Maire, S., Brun, C. et al. (2005) 'Protein interaction mapping: a Drosophila case study', *Genome Research* 15(3): 376-84.

Fremion, F., Astier, M., Zaffran, S., Guillen, A., Homburger, V. and Semeriva, M. (1999) 'The heterotrimeric protein Go is required for the formation of heart epithelium in Drosophila', *Journal of Cell Biology* 145(5): 1063-76.

Hornstein, N. J., Pulver, S. R. and Griffith, L. C. (2009) 'Channelrhodopsin2 mediated stimulation of synaptic potentials at Drosophila neuromuscular junctions', *J Vis Exp*(25).

Hummel, T., Krukkert, K., Roos, J., Davis, G. and Klambt, C. (2000) 'Drosophila Futsch/22C10 is a MAP1B-like protein required for dendritic and axonal development', *Neuron* 26(2): 357-70.

Katanaev, V. L., Ponzielli, R., Semeriva, M. and Tomlinson, A. (2005) 'Trimeric G protein-dependent frizzled signaling in Drosophila', *Cell* 120(1): 111-22.

Katanaev, V. L. and Tomlinson, A. (2006) 'Dual roles for the trimeric G protein Go in asymmetric cell division in Drosophila', *Proceedings of the National Academy of Sciences of the United States of America* 103(17): 6524-9.

Koch, I., Schwarz, H., Beuchle, D., Goellner, B., Langegger, M. and Aberle, H. (2008) 'Drosophila ankyrin 2 is required for synaptic stability', *Neuron* 58(2): 210-22.

Kopein, D. and Katanaev, V. L. (2009) 'Drosophila GoLoco-protein pins is a target of Galpha(o)-mediated G protein-coupled receptor signaling', *Molecular Biology of the Cell* 20(17): 3865-77.

Koval, A., Kopein, D., Purvanov, V. and Katanaev, V. L. (2010) 'Europium-labeled GTP as a general nonradioactive substitute for [(35)S]GTPgammaS in high-throughput G protein studies', *Analytical Biochemistry* 397(2): 202-207.

Lecuit, T., Brook, W. J., Ng, M., Calleja, M., Sun, H. and Cohen, S. M. (1996) 'Two distinct mechanisms for long-range patterning by Decapentaplegic in the Drosophila wing', *Nature* 381(6581): 387-93.

Mahr, A. and Aberle, H. (2006) 'The expression pattern of the Drosophila vesicular glutamate transporter: a marker protein for motoneurons and glutamatergic centers in the brain', *Gene Expr Patterns* 6(3): 299-309.
Mathew, D., Ataman, B., Chen, J., Zhang, Y., Cumberledge, S. and Budnik, V. (2005) 'Wingless signaling at synapses is through cleavage and nuclear import of receptor DFrizzled2', *Science* 310(5752): 1344-7.
Nishimura, Y., Applegate, K., Davidson, M. W., Danuser, G. and Waterman, C. M. (2012) 'Automated screening of microtubule growth dynamics identifies MARK2 as a regulator of leading edge microtubules downstream of Rac1 in migrating cells', *PLoS One* 7(7): e41413.
Packard, M., Koo, E. S., Gorczyca, M., Sharpe, J., Cumberledge, S. and Budnik, V. (2002) 'The Drosophila Wnt, wingless, provides an essential signal for pre- and postsynaptic differentiation', *Cell* 111(3): 319-30.
Pfeiffer, S., Ricardo, S., Manneville, J. B., Alexandre, C. and Vincent, J. P. (2002) 'Producing cells retain and recycle Wingless in Drosophila embryos', *Current Biology* 12(11): 957-62.
Pielage, J., Cheng, L., Fetter, R. D., Carlton, P. M., Sedat, J. W. and Davis, G. W. (2008) 'A presynaptic giant ankyrin stabilizes the NMJ through regulation of presynaptic microtubules and transsynaptic cell adhesion', *Neuron* 58(2): 195-209.
Pulver, S. R., Hornstein, N. J., Land, B. L. and Johnson, B. R. (2011) 'Optogenetics in the teaching laboratory: using channelrhodopsin-2 to study the neural basis of behavior and synaptic physiology in Drosophila', *Advances in physiology education* 35(1): 82-91.
Reichsman, F., Smith, L. and Cumberledge, S. (1996) 'Glycosaminoglycans can modulate extracellular localization of the wingless protein and promote signal transduction', *Journal of Cell Biology* 135(3): 819-27.
Schaefer, M., Petronczki, M., Dorner, D., Forte, M. and Knoblich, J. A. (2001) 'Heterotrimeric G proteins direct two modes of asymmetric cell division in the Drosophila nervous system', *Cell* 107(2): 183-94.
Schroll, C., Riemensperger, T., Bucher, D., Ehmer, J., Voller, T., Erbguth, K., Gerber, B., Hendel, T., Nagel, G., Buchner, E. et al. (2006) 'Light-induced activation of distinct modulatory neurons triggers appetitive or aversive learning in Drosophila larvae', *Current Biology* 16(17): 1741-7.
Strapps, W. R. and Tomlinson, A. (2001) 'Transducing properties of Drosophila Frizzled proteins', *Development* 128(23): 4829-35.
Zhang, B. and Stewart, B. (2010) 'Electrophysiological recording from Drosophila larval body-wall muscles', *Cold Spring Harb Protoc* 2010(9): pdb prot5487.
Zito, K., Parnas, D., Fetter, R. D., Isacoff, E. Y. and Goodman, C. S. (1999) 'Watching a synapse grow: noninvasive confocal imaging of synaptic growth in Drosophila', *Neuron* 22(4): 719-29.

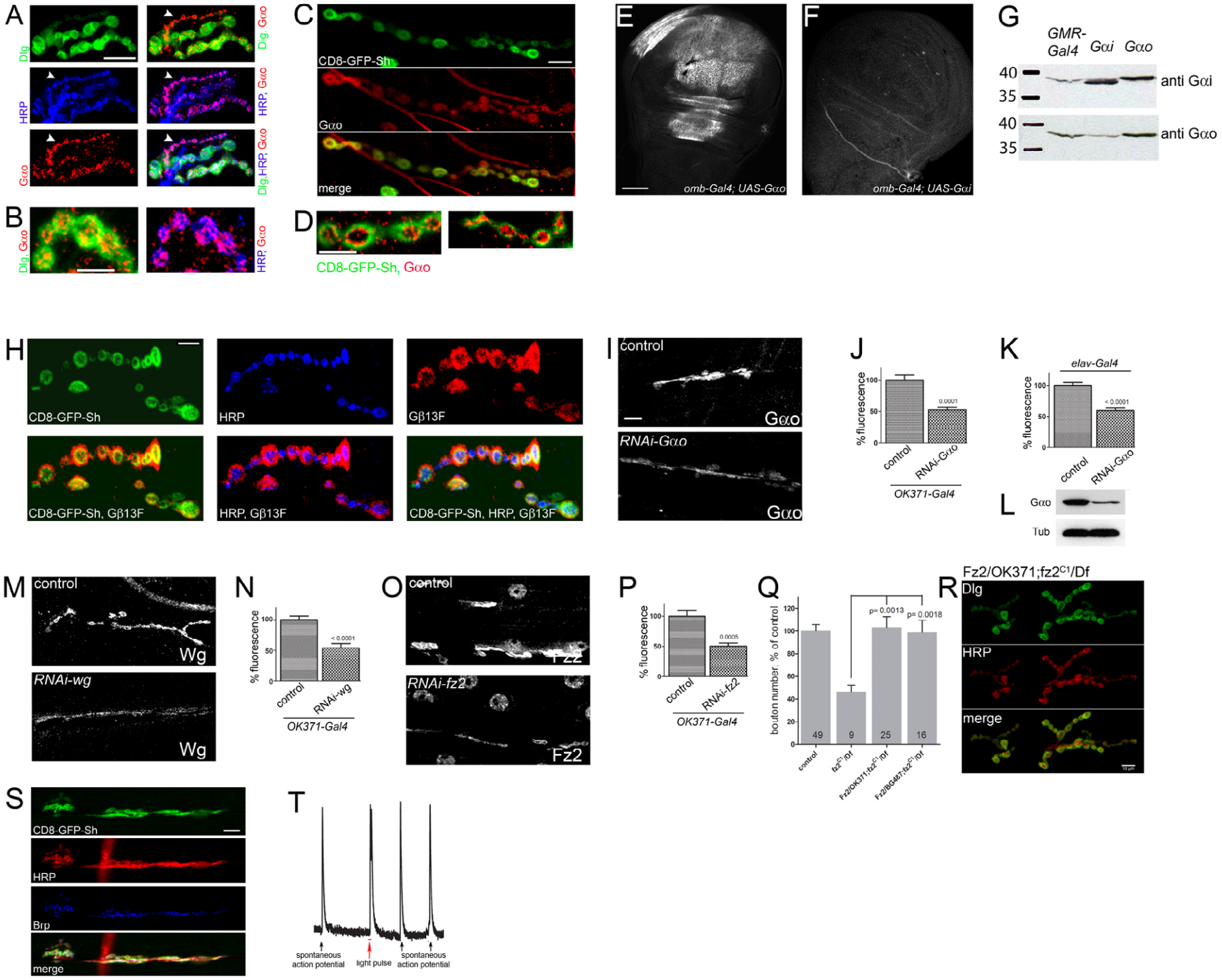
A
Dlg
Dlg, Gαo
HRP
HRP, Gαo
Gαo
Dlg,HRP, Gαo
B
Dlg, Gαo
HRP, Gαo
C
CD8-GFP-Sh
Gαo
merge
D
CD8-GFP-Sh, Gαo
E
omb-Gal4; UAS-Gαo
F
omb-Gal4; UAS-Gαi
G
GMR-Gal4
Gαi
Gαo
40
35
anti Gαi
anti Gαo
H
CD8-GFP-Sh
HRP
Gβ13F
CD8-GFP-Sh, Gβ13F
HRP, Gβ13F
CD8-GFP-Sh, HRP, Gβ13F
I
control
Gαo
RNAi-Gαo
J
% fluorescence
control
RNAi-Gαo
OK371-Gal4
K
elav-Gal4
L
Gαo
Tub
M
control
Wg
RNAi-wg
N
control
RNAi-wg
OK371-Gal4
O
control
Fz2
RNAi-fz2
P
control
RNAi-fz2
OK371-Gal4
Q
bouton number, % of control
p= 0.0013
p= 0.0018
49
9
25
16
R
Fz2/OK371;fz2C1/Df
Dlg
HRP
merge
S
CD8-GFP-Sh
HRP
Brp
merge
T
spontaneous action potential
light pulse
spontaneous action potential

Figure S1. Characterization of the anti-Gαo antibodies and the RNAi lines.

(A) Gαo (red) is expressed in the presynaptic side of NMJ and is barely detected postsynaptically, as judged by colocalization with anti-HRP (blue) but only partial overlap with Dlg (green). Arrowhead points to the types Is boutons depicting low anti-Dlg staining. Scale bar 10μm. (B) High-magnification anti-Dlg (green), -Gαo (red), and -HRP (blue) staining. Scale bar 5μm. (C) Rabbit polyclonal antiserum raised against recombinant *Drosophila* Gαo produces the same staining pattern as shown in Figure 1. Scale bar 10μm. (D) High-magnification CD8-GFP-Sh (green) and anti-Gαo (red) staining. Scale bar 5μm. (E, F) The *omb-Gal4* driver was used to overexpress *Drosophila* Gαo (E) or Gαi (F) in wing imaginal discs. The anti-Gαo antibodies (Merck, raised against the C-terminal peptide corresponding to human Gαo, used in Figure 1) recognized overexpressed Gαo in the characteristic *omb* domain. In contrast, Gαi was not detected even with enhanced microscope settings. Scale bar 50μm. (G) Western blot of fly head extracts (wild type or overexpressing Gαo or Gαi) probed with antibodies against Gαo or Gαi. The anti-Gαo antibodies (Merck) recognize only the higher-migrating Gαo, both endogenous and overexpressed. The anti-Gαi antibodies (Merck) recognize both *Drosophila* Gαo and Gαi; Gαi migrates lower than Gαo and is not detectable in the non-Gαi-overexpressing samples. (H) Gβ13F (red) is found both in the presynapse colocalizing with anti-HRP (blue) and in the postsynapse colocalizing with, and even expanding the domain of, CD8-GFP-Sh (green). Scale bar 5μm. (I) Immunostainings of the wild-type (control) and *RNAi-Gαo*-expressing NMJ driven with *OK371-Gal4* at muscle 6/7 performed in parallel and recorded with identical microscope settings show a clear although incomplete downregulation in the levels of the proteins. (J) Quantification of the mean fluorescence in the NMJ indicates a two-fold decrease of fluorescence levels. Scale bar 10μm. (K) Expression of *RNAi-Gαo* with the driver *elav-Gal4* leads to a comparable decrease of Gαo in the NMJ determined by quantification of mean fluorescence. Western blot of fly head extracts expressing *RNAi-Gαo* with *elav-Gal4* however clearly demonstrates a drastic decrease in protein levels (L). (M-P) *RNAi-wg* and *RNAi-fz2* driven by *OK371-Gal4* also result in a clear downregulation of the Wg (M, N) and Fz2 (O, P) proteins as judged by immunostainings and quantification of the fluorescence in the NMJ. Immunostaining and image acquisition was performed like in (I, J). Anti-Fz2 antibodies have immunoreactivity in the muscle nuclei; note similar nuclear postsynaptic signal in control and *RNAi-fz2* samples (O). (Q) Quantification of total number of boutons show a rescue of the *fz2* mutant phenotype both by presynaptic and postsynaptic overexpression. (R) Representative image of presynaptic Fz2 rescue. Scale bar 10 μm. (S) Expression of Ptx in motoneurons results in reduced bouton numbers and aberrant NMJ morphology, similar to the phenotype of loss of Gαo (see Figure 2C). Scale bar 10μm. (T) Examples of spontaneous action potentials (black arrows) generated in the same recording session as a light-induced action potential (red arrow). The EJP amplitude and duration of the light-induced and spontaneous action potentials are similar. Scale as on Figure1G.

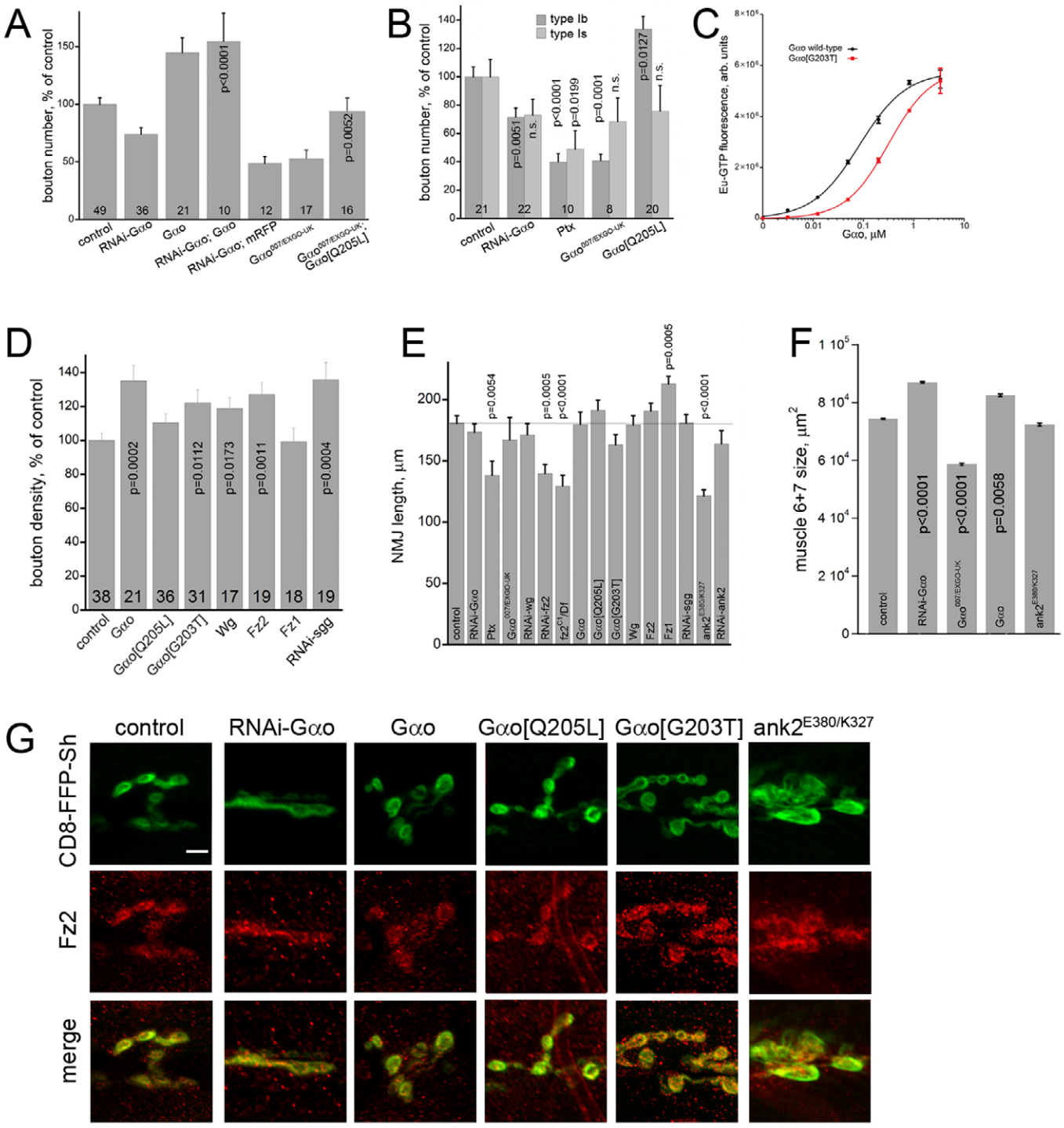

Figure S2. NMJ characterization and Fz2 localization in different genotypes; characterization of Gαo[G203T].

(A) The decrease of bouton number induced by downregulation of Gαo by RNAi is rescued by presynaptic co-overexpression of *Gαo* (p-value refers to the difference from *RNAi-Gαo*) to the level of *Gαo* overexpression. mRFP fails to restore bouton number of *RNAi-Gαo*. Pre-synaptic expression of activated Gαo rescues the *Gαo* genetic mutants (p-value refers to the difference from *Gαo*$^{-/-}$). (B) Change in type Ib and type Is bouton numbers upon alteration of Gαo levels or functionality. (C) Saturation binding curves of recombinant Gαo (black circles) and Gαo[G203T] (red squares) demonstrate that both proteins can be charged with Eu-GTP. Their affinities to the nucleotide analog differ, with that of the wild-type protein being about 4 times higher as judged by the calculated EC_{50} values of these proteins (83±8 nM for Gαo *vs* 316±37 nM for Gαo[G203T]). (D) Bouton density upon overactivation of the Wg pathway; p-values compared to the control are indicated. (E) Length of the NMJ of the indicated genotypes. (F) Muscle area of the indicated genotypes. p-values show significant differences to the control. (G) Localization of Fz2 in boutons of the denoted genotypes. Synaptic Fz2 localization is unaffected upon perturbations in Gαo or Ank2 levels. Scale bar 5μm.

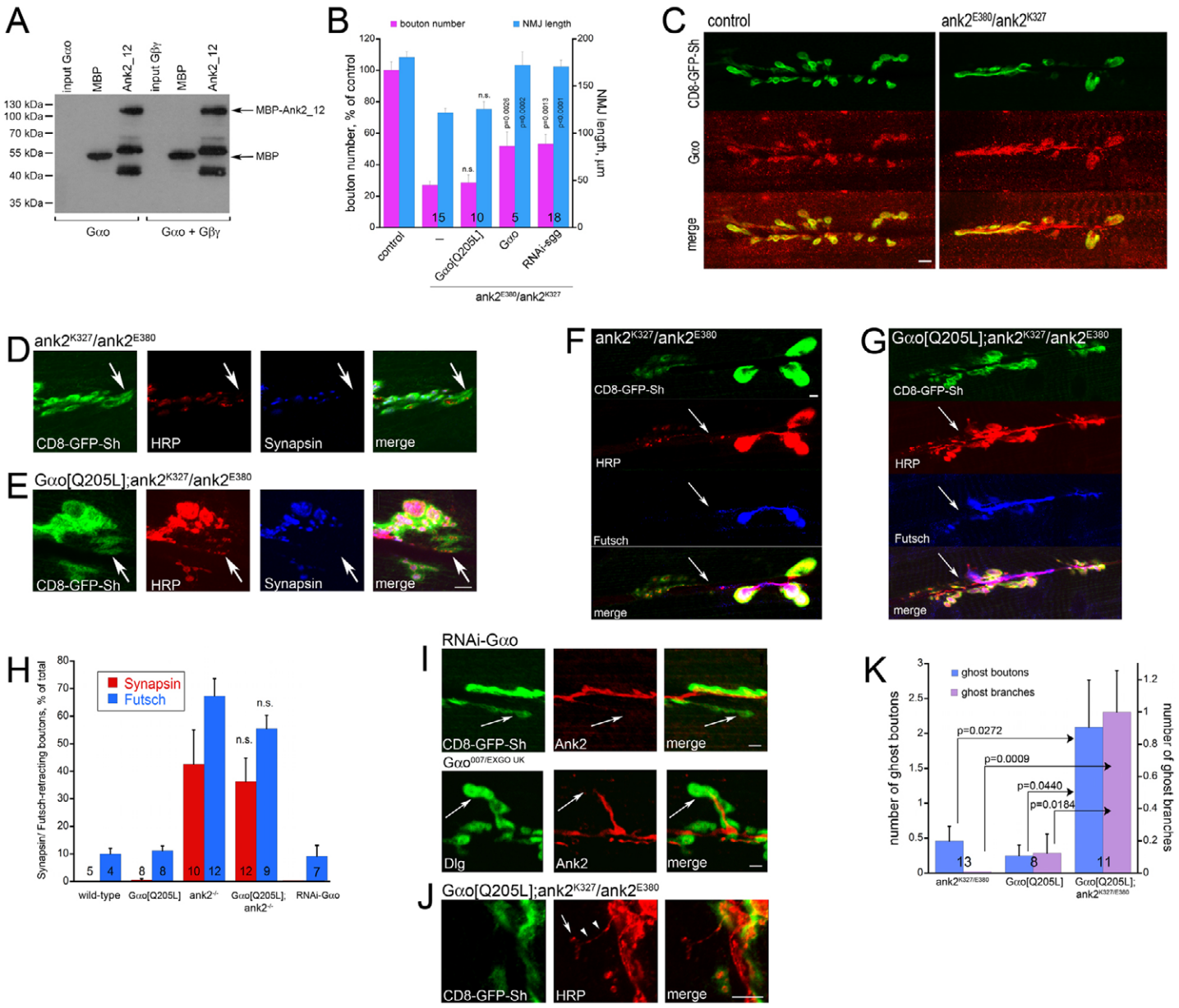

Figure S3. Additional controls to Western blotting, bouton quantification and analysis of presynaptic defects.

(A) Probing the western blot of Figure 5C with anti-MBP antibody demonstrates equal loading of the MBP control and MBP-Ank2_12. MBP-Ank2_12 is purified as a mixture of the full-length protein (ca. 120kDa) and two major degradation products. (B) Bouton number and NMJ length are increased in the *Gαo; ank2$^{E380/K327}$* and *RNAi-sgg; ank2$^{E380/K327}$* genotypes compared to *ank2$^{E380/K327}$*. Numbers of NMJ analyzed and p-values are indicated, n.s. means 'not significant'. (C) Synaptic Gαo localization is unaffected upon loss of Ank2. Scale bar 10 µm. (D-G) Synaptic retractions in *ank2$^{-/-}$* (D, F) or *ank2$^{-/-}$; Gαo[Q205L]* (E, G) seen at the level of synaptic loss of Synapsin (D, E) or Futsch (F, G). Arrows in (D, E) point to some boutons having HRP but no Synapsin staining. Arrows in (F, G) point to the "border" where Futsch staining starts to be lost. Scale bar 5 µm. (H) Quantitation of synaptic retractions in different genotypes. (I) Ghost boutons (arrow) in boutons that still present in RNAi-Gαo and Gαo mutant NMJs. Scale bar 5 µm. (J) Neuronal processes (arrowheads) containing presynaptic HRP but lacking the postsynaptic structures can be seen upon overactivation of Gαo in the absence of Ank2. Scale bar 5 µm. (K) represents quantification of the phenotypes.

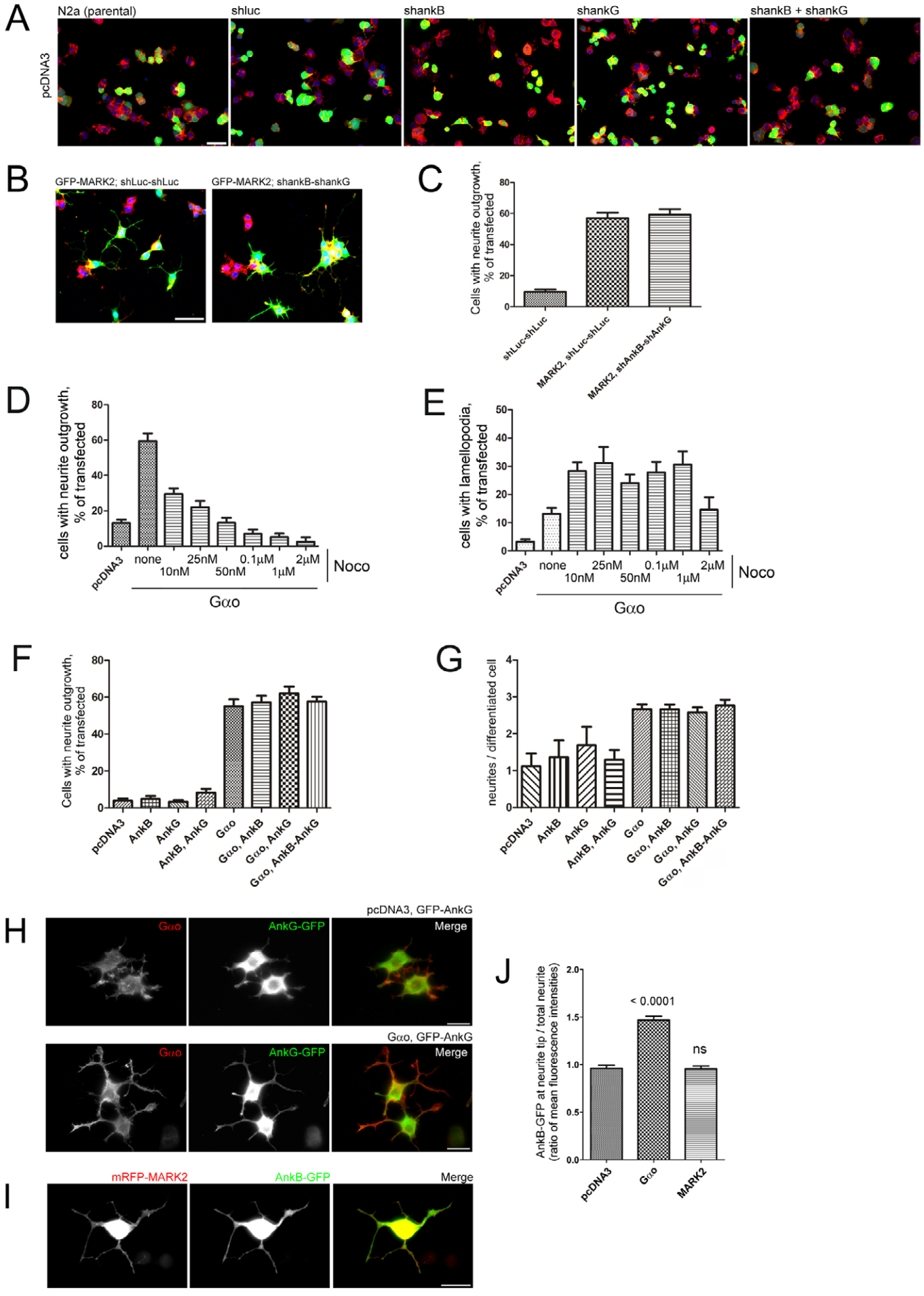
A
N2a (parental)
shluc
shankB
shankG
shankB + shankG
pcDNA3
B
GFP-MARK2; shLuc-shLuc
GFP-MARK2; shankB-shankG
C
Cells with neurite outgrowth, % of transfected
shLuc-shLuc
MARK2, shLuc-shLuc
MARK2, shAnkB-shAnkG
D
cells with neurite outgrowth, % of transfected
pcDNA3
none
10nM
25nM
50nM
0.1μM
1μM
2μM
Noco
Gαo
E
cells with lamellopodia, % of transfected
F
Cells with neurite outgrowth, % of transfected
pcDNA3
AnkB
AnkG
AnkB, AnkG
Gαo
Gαo, AnkB
Gαo, AnkG
Gαo, AnkB-AnkG
G
neurites / differentiated cell
H
pcDNA3, GFP-AnkG
Gαo
AnkG-GFP
Merge
Gαo, GFP-AnkG
I
mRFP-MARK2
AnkB-GFP
J
AnkB-GFP at neurite tip / total neurite (ratio of mean fluorescence intensities)
< 0.0001
ns
MARK2

Figure S4. N2a cell treatments.

(A) Transfection of parental N2a cells with pcDNA3 empty vector poorly induces formation of neurites and lamellopodia. shRNA-stably transfected control (shluc) as well as *ankB* (shankB) and *ankG* (shankG) single and double knockdowns do not show any apparent phenotype after pcDNA3 transfection. Co-expression of EGFP (green) shows transfected cells and Rhodamine phalloidin (red) and DAPI (blue) are used to visualize F-actin and nuclei, respectively. Scale bar: 20 mm. (B) Overexpression of EGFP-tagged MARK2 (GFP-MARK2) induced neurite outgrowth in control shRNA-transfected (shluc-shluc) cells which is not affected in *ankB/G* double know-down (shankB-shankG) cells. Scale bar: 50 mm. (C) Quantification of the experiment described in (B). (D-E) Quantification of the Nocodazole (Noco) effects on neurite outgrowth (B) and lamellopodia formation (C) in Gαo overexpressing N2a cells. Nocodazole treatment blocks neurite outgrowth in a concentration dependent manner (B), while formation of lamellopodia is increased at any Nocodazole concentration (C). (F-G) Quantification of the effects on neurite outgrowth and neurite per cells by the overexpression of EGFP-tagged *ankB* (AnkB-GFP) or *ankG* (AnkG-GFP) in combination with Gαo or empty pcDNA3 vector. (H) Representative images of N2a cells overexpressing AnkG-GFP alone (pcDNA3, AnkG-GFP) or together with Gαo (Gαo, AnkG-GFP). Red fluorescence indicates Gαo immunostaining. (I) No accumulation of AnkB-GFP in neurite tips (and a more homogeneous distribution along the whole of the neurite instead) was observed upon overexpression of an mRFP-tagged MARK2 (mRFP-MARK2) construct (cf. Figure 7J). Scale bar: 10µm. (J) Ratio values of mean fluorescence intensities of AnkB-GFP at neurite tips vs. whole neurites indicate that AnkB significantly accumulates at the rear end of neurites formed by Gαo overexpression, but not at spontaneously formed neurites (pcDNA3) or at neurites induced by mRFP-MARK2 co-expression. P-value (Students t-test) is shown for Gαo co-overexpression. ‘ns’: non-significant (P>0.05).